Cortical layer-specific modulation of neuronal activity after sensory deprivation due to spinal cord injury

Marta Zaforas[1,2,3], Juliana M Rosa[1,3], Elena Alonso-Calviño[1], Elena Fernández-López[1], Claudia Miguel-Quesada[1], Antonio Oliviero[2] and Juan Aguilar[1,4]✉.

[1]Experimental Neurophysiology and Neuronal Circuits Group, Research Unit, Hospital Nacional de Parapléjicos. SESCAM, Toledo, Spain.

[2]FENNSI Group, Research Unit, Hospital Nacional de Parapléjicos. SESCAM, Toledo, Spain.

[3]Equal contribution.

[4]Lead Contact

✉ Corresponding Author: Juan Aguilar, jdaguilar@sescam.jccm.es

Summary

Cortical areas have the capacity of large-scale reorganization following sensory deprivation. However, it remains unclear whether this is a unique process that homogenously affects the entire deprived region or it is suitable to changes depending on local circuitries across layers. By using *in vivo* electrophysiology to record neuronal activity simultaneously across cortical depth, we showed that sensory deprivation due to spinal cord injury induces layer-specific changes in both spontaneous and evoked-activity. While supragranular layers specifically increased gamma oscillations and the ability to initiate up-states during spontaneous activity, infragranular layers displayed increased, faster and delayed evoked-responses to sensory stimulation. Therefore, sensory deprivation immediately modifies local circuitries allowing supragranular layers to better integrate spontaneous corticocortical information to maintain column excitability, and infragranular layers to better integrate evoked-sensory inputs to preserve subcortical outputs. These layer-specific changes may guide long-term alterations in excitability and plasticity associated to network rearrangements and the appearance of sensory pathologies associated with spinal cord injury.

Introduction

Spinal cord injury (SCI) induces an abrupt and robust loss of sensory inputs onto cortical areas that receive information from body regions below the lesion level (i.e. hindlimb cortex that receives afferent inputs from hindlimbs). This sensory deprivation initiates the so-called process of cortical reorganization (CoRe), which is typically described as an expansion of the neuronal activity from intact cortical areas towards the sensory deprived cortex (Curt et al. 2002; Endo et al. 2007; Ghosh et al. 2010; Jain et al. 2008; Jain, Florence, and Kaas 1998). CoRe plays key roles in the functional recovery after SCI, but it has also been implicated in the generation of associated pathologies such as neuropathic pain and spasticity (Gustin et al. 2010; Peyron et al. 2004; Philip J. Siddall et al. 2003; Wrigley et al. 2009). Similar cortical rearrangements after sensory deprivation have also been described in different sensory systems as visual (Griffen et al. 2017; He, Hodos, and Quinlan 2006) and auditory cortex (Bola et al. 2017). Most of studies about cortical reorganization after SCI have used large-scale experimental approaches such as extracranial electroencephalographic recordings (Green et al. 1998), voltage sensitive dye (Ghosh et al. 2010) and functional magnetic resonance imaging (Endo et al. 2007) in a time period ranging from days-to-months after the injury. However, it is currently known that such functional changes are observed immediately after SCI in different animal models as rodents (Aguilar et al. 2010; Humanes-Valera, Aguilar, and Foffani 2013; Yagüe et al. 2014; Yague, Foffani, and Aguilar 2011) and pigs (Catherine R. Jutzeler et al. 2019). In this line, our group have previously shown that layer 5 neurons of both intact and deprived somatosensory cortex became more responsive to peripheral sensory stimulation above lesion level few minutes after the injury (Humanes-Valera, Aguilar, and Foffani 2013; Yagüe et al. 2014), while spontaneous activity is drastically reduced (Aguilar et al. 2010; Fernández-López et al. 2019). In addition to the cortical changes, SCI also modifies thalamic and brainstem spontaneous and evoked neuronal excitability, which may be linked to the changes observed in the somatosensory cortex (Alonso-Calviño et al. 2016; Dutta et al. 2014; Jain et al. 2000, 2008; Liang and Mendell 2013).

Changes in the cortical activity after SCI have been mostly studied by using electrophysiological recordings from layer 5 neurons. However, the neocortex is a complex structure composed of six layers organized in distinct vertical columns. Within each layer, different functional properties and input/output connections are achieved by interconnected excitatory pyramidal neurons, inhibitory neurons and glial cells (Bayraktar et al.,

2020; Derdikman et al., 2006; Fiáth et al., 2016; Tischbirek et al., 2019). Although several studies in the last decade have shed light into distinct strategies used by each layer to encode information, less is known about the functional changes induced within each cortical layer following sensory deprivation that may precede long-term cortical reorganization and could help to understand the physiological changes in brain areas controlling the integration and processing of sensory inputs.

Using *in vivo* electrophysiological recordings from anesthetized rats, we studied how neuronal activity mediated by corticocortical and thalamic connections as well as local circuitries in the hindlimb cortex (HLCx) are immediately affected by sensory deprivation after a thoracic SCI. For that, we used a vertical multielectrode array to determine the neuronal excitability across layers of the deprived HLCx during evoked and spontaneous activity. Peripheral stimulation of the contralateral forelimb showed homogenous increase in sensory evoked local field potential (LFP) responses across HLCx layers indicating that changes in neuronal network properties of the deprived cortical column may favour the excitability. However, a striking heterogeneity was observed when other physiological parameters were analysed. Infragranular L5/6, but not L2/3, exhibited increased LFP slope, multiunit activity and delayed onset latencies. Our data points to a direct effect of thalamocortical connections on the delayed onset as observed by simultaneous cortical-thalamic electrophysiological recordings. On contrary to evoked-responses, spontaneous activity was mostly affected in supragranular layers as observed by increased high-rhythms frequencies and probability of up-states initiation. Altogether, our data indicate that SCI immediately modifies local circuitries within the deprived cortex allowing supragranular layers to better integrate spontaneous corticocortical information, thus modifying the excitability of the column, and infragranular layers to better integrate evoked-sensory inputs to preserve subcortical outputs.

RESULTS

Laminar analysis of evoked neuronal responses in the somatosensory cortex following peripheral stimulation

We first characterized the evoked-local field potentials (evoked-LFP) across layers of the HLCx in response to sensory stimulation delivered either to the contralateral hindlimb (HL) or forelimb (FL) in intact anaesthetised animals (Fig. 1). For that, we used a linear 32-multielectrode probe inserted vertically into the HLCx such that recording sites were located across all layers in a single column to simultaneously record LFPs and local multiunit activity (MUA, Fig. 1A). Figure 1A shows a schematic representation of the recording location and stimulation paradigm as well as a histological preparation showing an electrode track into HLCx (Fig. 1B). Representative examples of averaged evoked-LFPs across the entire depth of HLCx in response to a 5 mA hindlimb stimulation (0.5 Hz) is shown in the left panel of Figure 1C. Note that a high intensity stimulation was chosen to maximize the activation of peripheral nerves to ensure the full engagement of cortical circuits involved in somatosensory processing (Lilja et al. 2006). The laminar profile of averaged LFP responses of the population obtained by hindlimb stimulation showed a clear difference in the response magnitude across the cortical depth, with a maximum peak at distances from surface between 700-1000 µm corresponding to the thalamorecipient granular layer 4. No differences were observed using low intensity stimulation, which resembles light mechanical stimuli that preferentially activates dorsal column pathways (Lilja et al. 2006). Current source density (CSD) analysis was overlapped to LFP traces to determine the entrance of synaptic inputs in different cortical layers (Fig. 1C, heat map) showing an evident current sink (inward current) in L4. The active sink was surrounded by two strong current sources (outward current), one short-lasting in L2/3 and another long-lasting in infragranular layers 5 and L6. A small and elongated current sink was also observed in L6, which may refer to the thalamocortical loop initiated by evoked responses. The greater LFP response magnitude and the current sink at the thalamorecipient L4 corroborate the correct location of the electrode at the somatotopic representation of hindlimbs. Finally, MUA responses (Fig. 1D, left panel) were analysed by rectifying the neuronal firing (rMUA) obtained in response to peripheral stimulation at high and low intensities (Fig. 1D, right panel). The area of the evoked-rMUA showed robust neuronal firing in the upper infragranular layer (i.e. L5), while L2/3 and L6 neurons showed low and sparse firing response. A similar laminar profile of neuronal responses was observed using low intensity stimulation (0.5 mA).

We next examined the pattern of cortical responses when the peripheral stimulation was applied to an adjacent, non-corresponding somatotopic body region, i.e. recording in HLCx, while stimulating forelimb afferents. Figure 1E shows LFP representative traces recorded from the HLCx in response to high intensity electrical stimulation of contralateral forelimb. Despite of the small amplitude, evoked-LFP responses were clearly observed across all recording channels with

infragranular layers showing the highest magnitude. Similar results were also observed using 0.5 mA stimulation indicating a strong HL-FL cortical connectivity even to low intensity stimuli. In response to high stimulation, rMUA in infragranular layers showed a clear evoked activity with a peak in layer 6, while L2/3 and L4 exhibited only sparse and very low response. Due to the non-consistent responses obtained among individuals when low intensity stimulation was applied, herein, data were considered only for responses obtained to high intensity stimulation in forelimb (5mA). Overall, our data indicate a layer-specific neuronal activity in the HLCx in response to either hindlimb or forelimb peripheral stimulation.

SCI induces layer-dependent functional changes in the sensory deprived cortex

Next, we investigated the neuronal responses across cortical layers immediately after sensory deprivation due to SCI (Fig. 2). As expected, an abolishment of the evoked-LFP was observed in all HLCx layers in response to hindlimb stimulation, confirming the complete loss of peripheral sensory inputs (Fig. 2A). On the other hand, SCI induced increased evoked-LFP in HLCx when peripheral stimulation was applied to forelimb (Fig. 2C, repeated measures ANOVA, SCI $F_{(1,91)} = 51.6$, $p < 0.001$). Although the averaged values were statistically different in most of the layers, visual inspection of our data pointed to a subset of individuals in which evoked-LFP were not affected by SCI, or even exhibited decreased amplitude (Sup. Fig. 1A). To confirm that, we conducted a covariance index (CVI) analysis to statistically determine the individuals exhibiting increased covariance of LFP responses before and after SCI (Sup. Fig. 1B). Following this analysis, we were able to classify individuals in two groups (Sup. Fig. 1B and Fig. 2B-D). Group 1 (CVI > 1) exhibited a homogenous increase of nearly 30% of the evoked-LFP across all layers after SCI (19 out of 24 animals, 79%), while Group 2 (CVI ≤ 1) was not affected by SCI (5 out of 24 animals, 21%). These results corroborate previous data in SCI patients and indicate that initiation of cortical changes after SCI depends on individuals (Freund et al. 2013; C. R. Jutzeler, Curt, and Kramer 2015).

Increased evoked-LFP responses after SCI could reflect changes in the excitatory post-synaptic activity of local pyramidal neurons and/or in the strength of arriving synaptic inputs. To better characterize the functional modifications of deprived cortical layers after SCI, we measured the slope of the evoked-LFP as the decay rate in mV/s (Fig. 2E). Under control conditions, hindlimb stimulation induced fastest responses in L4 of the HLCx (Sup. Fig. 2), while forelimb stimulation induced similar slope values across all layers (Sup. Fig. 2, Fig. 2F). After SCI, slope values significantly increased in HLCx L4 and infragranular layers in response to forelimb stimulation in Group 1 animals (Fig. 2F). The fastest rising slope was observed in L6 indicating a possible faster recruitment of neuronal population after SCI as can be observed by a shorter time-to-peak values (Fig. 2G). Together, these results indicate that each layer have distinct mechanisms that are immediately modulating the local neuronal network of the deprived sensory cortex.

In order to accurately determine whether immediate sensory deprivation induces heterogeneous functional changes in neuronal responses across HLCx layers, we examined the MUA patterns recorded in the two groups of animals (Fig. 3). For that, we used the area of the rectified MUA as a measure of local neuronal activity, as indicated in Fig. 3A. Figure 3B shows examples of evoked rMUA from each channel superimposed on a colour-coded map from the same animal in response to high intensity stimulation (5 mA) before and after SCI. Two-way analysis of variance of our data showed significant differences for layers ($F_{(3,59)} = 12.9$, $p < 0.001$), and SCI condition ($F_{(1,59)} = 18.95$, $p < 0.001$), but no interaction between layers and SCI condition ($F_{(3,59)} = 0.95$, $p = 0.42$). Before SCI, L2/3 and L4 neurons exhibited very low activity, while robust firing was observed only in L5 and L6 in response to forelimb stimulation. After SCI, neuronal firing increased in all layers but L2/3, being L5 rMUA statistically higher post-lesion ($p<0.05$). On the other hand, no changes in neuronal firing in Group 2 animals were observed (Fig. 3E-F). Taken together, these results demonstrate that immediate sensory deprivation due to SCI produces increased neuronal firing in infragranular layers, and importantly creates differences in neuronal excitability among cortical layers of the deprived HLCx.

SCI strongly affects the corticocortical connectivity between infragranular layers

To better understand the layer-dependent effect of sensory deprivation, response latencies were determined for each electrode site and for spatially averaged responses within electrodes from the same layer to create a spatiotemporal profile of the response onset (Fig. 4). Onset responses from LFP and rMUA were obtained by fitting a sigmoid function to the data and then computing the maximum curvature as described in (Fedchyshyn and Wang 2007; see Methods). Figure 4A-B shows an example of laminar LFP profile and averaged onset latencies obtained from HLCx in response to hindlimb stimulation in control conditions. In this case, activity originated in upper middle layers and spread upwards and downwards resembling the

propagation of evoked activity typically seen in distinct cortices (Sakata and Harris 2009; Schroeder, Mehta, and Givre 1998). Next, we analysed the evoked-LFP onset in response to forelimb stimulation, which could indicate how the corticocortical connectivity between HL-FL cortices is organized. In both groups of animals (Fig. 4C-D pre-SCI, Sup. Fig. 2D), averaged onset was found to be similar across all layers with higher probability to be initiated in infragranular layers. These data indicate that population activity measured as LFP in response to peripheral forelimb stimulation reaches HLCx almost simultaneously as previously reported using voltage-sensitive dyes (Wester and Contreras 2012). Such pattern of activity onset was strongly affected by sensory deprivation in a layer-dependent manner. Infragranular layers presented a significant delay in the onset of the evoked responses, while onsets in granular and supragranular layers were not affected (Fig. 4C-D). In addition, onset probability was also similar across layers after SCI. We then analysed the onset pattern of the evoked rMUA (Fig. 4E). Before SCI, HLCx infragranular layers exhibited faster onset latencies than supragranular layer with neuronal firing originating mostly in infragranular layer 6. After SCI, differences in onset responses disappeared (Fig. 4E) due to rMUA of infragranular neurons tended to be delayed.

Sensory information arrive to cortex by two different pathways

A possible mechanism leading to the delayed LFP and rMUA onsets in infragranular layers could be that SCI induces changes in the two main neuronal pathways that drive the peripheral information from forelimbs to HLCx: 1) a canonical corticocortical pathway in which synaptic inputs from the thalamic forelimb region routes to FLCx and then reaches HLCx mostly through L2/3 (FL-Th→FLCx→ HLCx); and 2) a non-canonical thalamocortical pathway involving the activation of a subset of HL neuronal population in the thalamus that project to HLCx in response to forelimb stimulation, HL-Th→HLCx (Figure 5A; Alonso-Calviño et al. 2016; Francis, Xu, and Chapin 2008). Taking into account that delayed onset were observed in both HL and FL thalamus immediately after SCI (Alonso-Calviño et al. 2016), we wanted to determine which thalamocortical pathway was the most probably to be involved in the delayed HLCx evoked-responses. Thus, if increased response latencies of HLCx after SCI were induced by changes in the canonical pathway, then synaptic inputs must arrive earlier at the FLCx than at HLCx. On the other hand, if non-canonical pathway produces the longer latency of HLCx evoked responses, then both cortical regions should exhibit similar latencies after forelimb stimulation. To prove this idea, we analysed simultaneous electrophysiological recordings from FLCx and HLCx obtained from tungsten electrodes located on layer 5 of both cortical regions under control conditions and after SCI (Fig. 5B, these data were obtained simultaneously to thalamic data that were published in Alonso-Calviño et al. 2016). Our results demonstrated that both the intact FLCx and the sensory deprived HLCx showed similar increased latencies to peripheral FL stimulation immediately after SCI with no differences between them (Fig. 5C, $p > 0.05$). Therefore, increased latency of cortical evoked responses could be, at least in part, due to longer latencies that take place in thalamic VPL corresponding to HL and FL as we described in Alonso-Calviño et al. 2016. Moreover, we cannot discard other intrinsic properties or corticocortical mechanisms involved in this process.

Spontaneous activity is determined by cortical layer properties under control conditions and after sensory deprivation

Cortical spontaneous activity in anesthetized animals is generally dominated by slow-wave activity (SWA, Fig 6A). SWA is mainly originated from local neuronal networks and corticocortical connections (Chauvette, Volgushev, and Timofeev 2010; Sanchez-Vives and McCormick 2000) and is importantly modulated by sensory inputs reaching the cortex throughout thalamic pathways (David et al. 2013; Rigas and Castro-Alamancos 2009). In this context, we have previously demonstrated that the drastic sensory loss after SCI reduced the neuronal excitability during cortical SWA (Aguilar et al. 2010; Fernández-López et al. 2019). As these data were obtained from deprived HLCx layer 5 neurons and SWA up-states propagate vertically across layers *in vitro* and *in vivo* (Sakata and Harris 2009; Sanchez-Vives and McCormick 2000), we thus calculated the onset of the spontaneous activity to determine the pattern of vertical propagation in our experimental conditions. Before SCI, spontaneous up-states initiated in any cortical layers (Fig. 6B), with infragranular layers 5 and 6 showing the highest onset probability (~80%), corroborating previous findings in somatosensory cortex of anesthetized rats (Fiáth et al. 2016; Sakata and Harris 2009). After SCI, we found that although spontaneous up-states also tend to start in infragranular layers, this probability decreased to ~60%. This effect was achieved by a parallel increase in the probability of up-states starting at L2/3. By analysing the rate of neuronal activity transfer across layers, we observed that up-states originated in L2/3 propagated downwards in similar velocities before and after SCI (Fig. 6C-D, control 38.7 ± 8.6 μm/ms, SCI 36.8 ± 11.2 μm/ms), whereas

spontaneous activity originated in deep layers propagated upwards in a velocity rate much slower after SCI than in control conditions (Fig 6E-F, control 39.2 ± 10.4 μm/ms, SCI 27.52 ± 12.1 μm/ms, $p < 0.01$). These data indicate that SCI induced immediate changes in the neuronal network of the deprived cortical column that slow-down the propagation of spontaneous activity originated in infragranular layers. In addition, they also showed an increased probability of spontaneous up-states initiated in L2/3, most probably through corticocortical connections between HL-FL that helps to propagate spontaneous activity from the adjacent FL cortex.

Changes in the generation of spontaneous activity may indicate that other cortical features could be affected by SCI. Following this idea, we considered that alterations of intrinsic excitability should also be reflected in the frequencies content of the LFP signal in each layer during spontaneous activity (Fig. 7). Spectrogram analysis performed on individual traces from L2/3, L4 and L5/6 layers (exampled red traces on Fig. 6A) confirmed the presence of slow (0.1-9 Hz) and fast rhythms (10-80 Hz) during up-states (Fig 6B). Interestingly, increased relative power of fast rhythms mainly in supragranular layers was observed following immediately after SCI. Changes in the internal frequencies within up-states can be clearly observed by the fast oscillations (band pass filtered 25-80Hz) shown in the original traces in Figure 6C (lower traces). To explore such frequency differences in a systematic manner, we performed a power spectrum analysis of the LFP frequencies that were divided into SWA (0.1-1 Hz), delta (1-4 Hz), theta (4-8 Hz), alpha (8-12 Hz), beta (12-25 Hz), low gamma (25-50 Hz) and high gamma (50-80 Hz). Our data showed that from all the studied frequency bands, the relative power of the high gamma was consistently increased in supragranular layers following a SCI (Fig. 6D). The rest of the studied frequency bands were not altered by SCI as summarized in Supplemental Table 3. Therefore, sensory loss produces changes in the intrinsic excitability of cortical layers characterized by lower ability of layer 5 to generate up-states and increased gamma frequency in supragranular layers during spontaneous activity.

DISCUSSION

Here we investigated the immediate effects that a robust sensory deprivation induces in distinct layers of the primary somatosensory cortex. Our study gives strong evidence that acute SCI induces layer-dependent changes in local circuits mediating evoked and spontaneous activity in the deprived cortical region through alterations of both corticocortical and thalamocortical connections. Regarding evoked responses, sensory deprivation potentiated the response magnitude and the rising of the population neuronal activity of infragranular layers (L5/6) of the deprived HLCx. On the other hand, the study of spontaneous activity show that supragranular layer 2/3 is the most affected by SCI exhibiting increased probability to initiate spontaneous up-states and increased power of high-frequency oscillations in the gamma band spectrum. Therefore, our results show that local neuronal and network properties of each cortical layer are responsible for differential effects observed in the deprived somatosensory cortex after SCI.

Layer-dependent changes in sensory-evoked responses after SCI

Sensory deprivation has dramatic effects on the organization of brain circuitries, leading to a takeover of the deprived cortex by other cortical areas. This process initiates as soon as deprivation occurs (Han et al., 2013; Humanes-Valera et al., 2013) and continues in a time scale from days-to-months (Endo et al., 2007; Sydekum et al., 2014; Humanes-Valera et al., 2017; Fernández-López et al., 2019). In the case of SCI, the reorganization of the deprived cortex leads to the acquisition of new sensory functions that could help functional recovery (Rossignol and Frigon, 2011) as well as initiates associated pathologies as pain and spasticity (Siddall and Loeser, 2001). The mechanisms driving beneficial or detrimental reorganization are unknown, but it could rely on the complex laminar organization of cortical areas known to have distinct cellular composition and intrinsic circuitries. Therefore, a better knowledge of the contribution of each cortical layer to the well-known phenomenon of CoRe after sensory deprivation is required. In this study, we have included for the first time the perspective of cortical layering role in the cortical changes after SCI, which could explain initiation and complexity of CoRe as well as explain the variability between individuals as observed in human patients.

Previous differences among layers were only addressed in a neonatal SCI model in which the effects of exercise in the cortical long-term plasticity were studied (Kao et al., 2009). Our present data goes further to demonstrate that neuronal activity is differentially affected across layers of the sensory-deprived HLCx immediately after a SCI in adult individuals. Under our experimental conditions, a homogenous increase in the magnitude of evoked-LFP in response to stimulation of the contralateral forelimb was observed across layers of the deprived cortex, which is very consistent with results

obtained using brain scanning approaches (Endo et al., 2007; Ghosh et al., 2010). This effect could be explained by the anatomical and functional overlapping of hindlimb and forelimb cortical areas (Moxon et al., 2008; Kao et al., 2009; Morales-Botello et al., 2012), in which corticocortical excitatory inputs may became unmasked following SCI and increases the responses to stimulation of non-corresponding extremity (i.e. forelimb). In addition, we have previously shown that SCI increases neuronal responses in the thalamic hindlimb region to forelimb stimulation (Alonso-Calviño et al., 2016). Therefore, changes in thalamic excitability could also play a direct role in the increased cortical responses of sensory deprived HLCx. On contrary to the homogenous increase in the magnitude of LFP responses across layers after SCI, the initial slopes of evoked-LFP were significantly faster in granular and infragranular neurons. Slope values are often used to determine changes in the arrival and/or synchronization of synaptic inputs and are usually affected by changes in the excitation:inhibition balance. Since cortical layers are known to display different inhibitory features (Wilent and Contreras, 2004), our data showing changes in the LFP slope in a layer-dependent manner suggest that local network properties are differentially affected by SCI and could represent an unequal reduction of local inhibition across layers allowing infragranular cells to better integrate evoked-sensory inputs.

Onsets of evoked-sensory responses in cortical regions are driven by synaptic inputs from corticocortical and thalamocortical connections. Our data shows almost simultaneous initiation of evoked responses between layers (Fig. 4C-D), corroborating *in vitro* data showing that horizontal corticocortical connectivity with adjacent cortical areas induces similar onsets of evoked responses (Wester and Contreras, 2012). However, this feature was strongly delayed in L5/6 of the deprived cortex after SCI, which could indicate modifications in the cortico-cortical synaptic connectivity but also in thalamic connections that project to HLCx. *In vivo* peripheral forelimb stimulation induces strong neuronal responses in the FL area of the thalamic VPL, but also in a population of the HL area of the VPL through collaterals (Alonso-Calviño et al., 2016) that finally project onto HLCx (Fig. 5A, Alonso-Calviño et al., 2016). By simultaneously recording neuronal activity in HLCx and HL thalamus we showed that SCI leads to a delayed latency in the neuronal activity of both regions in response to peripheral stimulation. In addition, we did not observe changes in the onset of thalamus-devoid supragranular neurons after SCI, suggesting that the onset of evoked-LFP responses in infragranular layers is more conditioned by changes in thalamic inputs. Therefore, our data indicate that although a delay in the arrival of synaptic inputs in infragranular layers is observed after SCI, these are more efficiently integrated as showed by increased slope and magnitude of evoked-LFP. Then, sensory deprivation produces changes in the integration properties of local networks of the deprived infragranular neurons that could be the basis for the long-term reorganization of sensory cortex observed after SCI.

Electrophysiological recordings of LFP and action potentials reflect different but complementary aspects of neuronal processing (Buzsáki et al., 2012). While LFP integrates subthreshold activity as synaptic inputs and membrane potentials from a neuronal population in a given local cortical region, action potentials are the output signals from individual neurons of a reduced area close to the recording electrode. Contrary to the homogeneous increased in the evoked-LFP after SCI, we found striking differences among layers regarding MUA. In this case, sensory deprivation increased neuronal activity in infragranular neurons of the deprived HLCx but not in granular and supragranular layers. Infragranular neurons have several characteristics that may lead to most of the changes: they receive excitatory inputs from all other cortical layers and neighbouring cortical areas (Schubert et al., 2007), they receive extensive thalamic inputs, and they have larger receptive fields (Moxon et al., 2008; Rigas and Castro-Alamancos, 2009; De Pasquale and Sherman, 2011; Wester and Contreras, 2013). Therefore, changes in the local network connectivity and/or intrinsic properties of infragranular neurons are more prone to be noticed after SCI compared to other layers. Moreover, the only intracellular data obtained from neuron of infragranular layers under same conditions of acute spinal cord injury (Humanes-Valera et al., 2017) perfectly support the relation between the increased MUA responses and the faster slope of evoked-LFP that we show in the present work. Altogether our data strongly indicates that activity of infragranular neurons are mostly affected in the context of evoked responses, which could be directly implicated in the mechanisms regulating subcortical output generating adequate behaviour and functional recovery following spinal cord injury.

Sensory deprivation affects the generation of gamma oscillations and the propagation of Up-states in the cortical column.

In our experimental model, the cortical activity before SCI was settle to the state of slow-wave oscillation (~1 Hz) characterized by alternating periods of synchronized activation of neuronal

population (up-states) and silent periods (down-states; Steriade et al., 1993). Up-state events are dominated by gamma frequency activity (25-80 Hz) with implications in multiple aspects of information processing such as sensory representation (Castro-Alamancos, 2009), sensorimotor integration (Schoffelen et al., 2011) and cognition (Gruber et al., 2004). Here, we describe that sensory deprivation due to SCI induces a layer-specific modulation of high frequency oscillations during Up-states, with gamma range being strikingly increased in supragranular layers, but not in infragranular or granular layers. Layer 2/3 is known to present a network of inhibitory neurons that initiates gamma-oscillations either through PV-neurons (Cardin et al., 2009; Welle and Contreras, 2016) or somatostatin neurons (Veit et al., 2017). In this context, the sensory deprivation produces a reduction in the constant thalamic excitatory inputs onto the deprived cortex that may lead to an increase of the general inhibitory tone in supragranular layers which facilitates local mechanisms of gamma oscillations. In addition to the well-described role of high frequencies in information processing, gamma oscillations have also been implicated in the formation of cortical maps during development (Minlebaev et al., 2011) and related to generation of pain perception in somatosensory cortex (Tan et al., 2019). Therefore, it is plausible that the increased gamma may be related with several long-term physiological changes observed following SCI such as cortical reorganization linked to functional recovery as well as maladaptive plasticity linked to chronic pain. Moreover, this neuronal feature could also be used as a functional biomarker for CoRe after a CNS injury, as previously shown in human auditory cortex after noise trauma (Ortman et al., 2010).

Spontaneous up-states within slow-wave oscillations usually initiate in deep infragranular layers (Sakata and Harris, 2009) and depend primarily on both intrinsic properties of the cortical column and corticocortical connections (Sanchez-Vives and McCormick, 2000; Timofeev et al., 2000). Our data shows that SCI induces a 1-fold increase in the probability of up-states generation in layer 2/3 with a consequent decrease in layers 5/6. There are several possible mechanisms that both isolated or synergistically could be leading to such changes. First, subthreshold oscillations in the membrane potential during gamma oscillations facilitate the generation of spontaneous up-states (Kuki et al., 2015, Puig et al., 2008). Since we also observed increased gamma in L2/3 after SCI probably due to increased activity of inhibitory neurons, this mechanism could be a trigger to the increased up-state onset (Compte et al., 2003). Second, we have previously shown that SCI decreases neuronal activity during up-states in layer 5 neurons (Fernandez-Lopez et al., 2019), which may favour the initiation of up-states in layer 2/3 by releasing supragranular neurons from L5 to L2/3 modulation (Wester and Contreras, 2012). In the same way, *in vitro* experiments show that up-states generation in the somatosensory cortex is reduced after blocking thalamocortical inputs, while a reduction of the fast excitatory activity (mediated by AMPA receptors) increases the probability to generate up-states in cortical layers 2/3 (Favero and Castro-Alamancos, 2013). Finally, the superficial cortical layer 2/3 is also known to receive long-range axons from other cortical areas that facilitate long-range synchronization (Yamashita et al., 2018). We have previously shown that SCI induces neuronal changes not only in the deprived HL cortex, but also in the adjacent, intact forelimb cortex (Humanes-Valera et al., 2017; Humanes-Valera et al., 2013). Therefore, changes in oscillatory synchronization in the sensory forelimb cortex may be transfer to hindlimb cortex through L2/3 corticocortical connections during spontaneous activity facilitating the up-state generation within the deprived cortical column. Despite of the mechanism used by the deprived cortex to generate spontaneous activity and to propagate the neuronal information across layers, the increase in L2/3 up-states may allow the deprived column to maintain its internal activity with possible implications in the processing of evoked sensory inputs as well as the reorganization of cortical areas after sensory deprivation.

Taking our results in the perspective of the long-term physiological effects that a SCI produces in the somatosensory cortex, it has been described how functional changes known as cortical reorganization can benefit functional recovery or can develop some pathophysiological consequences (as neuropathic pain). There are two main factors involved in development of the CoRe: 1) structural changes of neuronal networks and connections linked to anatomical rewiring of axons and dendrites, and 2) functional changes linked to activity-dependent plasticity and/or homeostatic plasticity (Muret and Makin, 2020). Since our results were obtained in a narrow time window (from minutes to few hours after deprivation), the possibility of structural and/or anatomical changes is limited. In this context, we have found in our results a subset of animals (21%) that consistently didn't show immediate neuronal changes related to evoked responses of spontaneous activity. This can be due to the short-term of observation, as experimental models describe how different changes take place in different time-windows after injury (Moxon et al 2014; Jutzeler et

al 2019). At the same time, this result can be consistent with a part of patients with SCI that are not affected at the sensorimotor cortical level (Moxon et al 2014). We found these results very important as they increase the variability and heterogeneity of effects observed in individuals with SCI, which should be taken into account in the context of cortical reorganization. however, the main results that we describe in this work are supported by the consistent effects observed in the 79% of animals with SCI that we have studied.

Neurons in the thalamocortical and corticocortical networks are not directly linked to spinal cord, except for a subset of corticospinal neurons of layer 5 in HLCx that when directly axotomized could be related to a reduction of firing rate observed during up-states of spontaneous activity (Fernández-López et al., 2019). On the contrary, we consider that the observed neuronal network alterations in a specific layer will depend on the importance of lacking preferred connectivity (thalamocortical or corticocortical), the inhibitory neuronal composition and how the network starts to integrate secondary/non-preferential and weak connections (as described in Muret and Makin, 2020). Then, immediate functional changes described in our results point to an initiation of homeostatic processes intended to compensate inputs deprivation by rebalance excitation:inhibition as it has been described in other sensory systems (Keck et al., 2013; Barnes et al., 2017; Teichert et al., 2017), which can be followed in the long-term by a process of activity-dependent plasticity. We found our results consistent with other models of deprivations as amputation (Makin et al., 2012), in which has been described that the map remains stable, but the function is affected. Importantly, our work provides a new framework for a better understanding of CoRe after SCI. Thus identifying a role for deprived supragranular layers in better integrating spontaneous corticocortical information to modify the excitability of the column, and the deprived infragranular layers in better integrating evoked-sensory inputs to preserve specific corticothalamic and cortico-subcortical networks. We postulate that the layer-specific neuronal changes observed immediately after sensory deprivation may guide the long-term alterations in neuronal excitability and plasticity linked to the rearrangements of somatosensory networks and the appearance of central sensory pathologies usually associated with SCI.

ACKNOLEDGEMENTS

We thank Dr. Casto Rivadulla for helpful comments on the manuscript. This work was supported by Ministerio de Economía y Competitividad and Ministerio de Ciencia, Innovación y Universidades, Spanish Government, BFU2016-80665-P and PID2019-105020GB to J.A., SAF2016-80647-R to A.O., both co-funded by FEDER; European Union's Horizon 2020 research and innovation programme under the Marie Sklodowska-Curie grant agreement No 794926 to J.M.R. and predoctoral fellowship FPI-MICINN from the Ministerio de Ciencia, Innovación y Universidades, Spanish Government BES2017-082029 to M.Z.

AUTHOR CONTRIBUTIONS

Conceptualization, J.A.; Methodology, M.Z., J.M.R., C.M., E.A., E.F., J.A.; Investigation, M.Z., J.M.R., C.M., E.A., E.F.; Original Draft, J.M.R., J.A., M.Z.; Writing–Review & Editing, M.Z., C.M., J.M.R., E.A., E.F., A.O., J.A.; Visualization, M.Z., J.M.R., J.A.; Funding Acquisition, J.M.R., J.A., A.O.

Declaration of Interests

The authors declare no competing interests.

FIGURE TITLES AND LEGENS

See Figures Sections

METHODS

Experimental approach

Experiments were performed on Wistar rats in accordance with the International Council for Laboratory Animal Science and the European Union 2010/63/EU guidelines. The experimental protocol was approved by the Ethical Committee for Animal Research at the Hospital Nacional de Parapléjicos (Toledo, Spain). Subjects were housed 2 per cages in standardized cages, with *ad libitum* access to food and water and maintained at 23 °C on a 12-hour light/dark cycle. A total of 24 male rats (range: 300-450 g; mean ± standard error of the mean, SEM: 400 ± 9.5 g) were used.

The general experimental approach (anaesthesia, surgery and peripheral stimulation) was similar to that used in our previous studies (Aguilar et al. 2010; Alonso-Calviño et al. 2016; Humanes-Valera et al. 2017; Humanes-Valera, Aguilar, and Foffani 2013). Briefly, animals were anaesthetised with an intraperitoneal injection of urethane (1.5 g/kg i.p.), placed in a stereotaxic frame (SR-6 Narishige Scientific Instruments, Tokyo, Japan) passively ventilated at 2 l O_2/min by a mask (Medical Supplies & Services, INT. LTD., England) and body temperature kept constant at 36.5ºC using

a homeothermic blanket (Cibertec SL, Madrid, Spain). Then, lidocaine 2% was applied subcutaneously into the areas of the incision and thoracic laminectomy (at T9–T10 vertebra) was performed keeping the dura mater intact and protected until the moment of performing a complete transection of the spinal cord. Next, the skull was exposed and a craniotomy was performed on the right hemisphere over the hindlimb representation of the primary somatosensory cortex (AP 0 to -3 mm; ML 1 to 4 mm) (Chapin and Lin 1984; Paxinos and Watson 2007) to allow lowering a vertical array for further record of neuronal activity. The stability of recordings was improved by drainage of the cisterna magna. The exact location of the probe was optimized by assessing the responses to tactile stimulation of the rat´s hindlimb with a cotton swab while listening to the recorded signal through a pair of loudspeakers.

Electrophysiological recordings and peripheral stimulation

Extracellular recordings were obtained by a linear vertical probe of 32 iridium contacts with diameter 177 μm^2 spaced at 50 µm (impedance 1-4 MΩ at 1 kHz; NeuroNexus Technologies Inc., US). The array was slowly introduced (1-2 µm/s) through the craniotomy into the HLCx (Fiáth, Márton, et al. 2019) and a ground electrode was placed in the parietal muscular tissue. The reference electrode was built in the vertical probe, 0.5 mm above the superficial recording site and outside the cortex (diameter 4200 μm^2). Recording protocol started ~40 min after the end of the electrode insertion to allow recovery of cortical tissue following time line in Figure 1A. Spontaneous activity was recorded during 10 min. Stimulation protocol (0.5 ms pulse duration at 0.5 Hz) was applied through bipolar needle electrodes located subcutaneously in the wrist of contralateral forelimb and hindlimb extremities. Two different intensities were applied: 1) low intensity (0.5 mA) to activate only a fraction of the available peripheral fibres, mainly low-threshold primary fibres running through the lemniscal pathway, from the dorsal column to the brainstem, and 2) high intensity (5 mA) to activate the maximum number of fibres including high-threshold primary fibres that synapse in the dorsal horns of the spinal cord including the spinothalamic tract (Lilja et al. 2006; Yague, Foffani, and Aguilar 2011). After recordings of evoked and spontaneous activity in control conditions, complete transection of the spinal cord was performed using a spring scissors. Immediately after transection, pulses of 10 mA electrical stimulation were applied to the contralateral hindlimb to confirm that no physiological responses were evoked by stimuli delivered below the level of the lesion. Complete spinal cord transection was also visually confirmed under the surgical microscope by the total separation of the borders. Recordings were continuously acquired during the transection to confirm the stability of the recordings. Approximately 20-30 min after the transection, the same protocol as before SCI was applied. Based on the absence of reflexes to forelimb stimuli, spontaneous whisker movements and corneal reflex, animals never received additional anaesthesia between the pre lesion protocol and the post lesion protocol. All recording data were converted into digital data at a 40 kHz sampling rate (16/24 rats) and 1kHz (8/24 rats), with 16–bit quantization by an OmniPlex System controlled by OmniPlex Server and PlexControl software (Plexon Inc, Texas, USA). All the 40 kHz signals were offline filtered (Spike2.v7, Cambridge Electronics Design, Cambridge, UK) into two signals: local field potentials (LFP, low-frequency band: up to 1kHz) and multiunit activity (MUA, high-frequency band: 0.3-3kHz).

Data analysis: evoked responses and spontaneous activity

For laminar profile analysis, LFP evoked responses from each electrode were averaged across 100 stimuli (0.5 Hz) and measured as the maximum amplitude to negative peak (mV) in the local fast response in a time window corresponding to 5-60 ms or 5-30 ms following sensory stimulation of hindimb or forelimb, respectively. In order to quantify MUA, the filtered recordings were rectified (rMUA) and averaged across 100 stimuli to measure the total voltage resulting from the averaged area of responses (µV). The obtained value was then subtracted from the background voltage obtained 50 ms before stimulation. For layer analysis, LFP from electrodes within the same layer were obtained according to the depth: layer 2/3 (150-650 µm), layer 4 (700-1000 µm), layer 5 (1050-1450 µm) and layer 6 (1500-2000 µm; Fiáth et al. 2016). In the case of rMUA, neuronal signals obtained from individual channels within a layer were summed up to allow robust detection of the neuronal activity.

Onset latency of evoked-LFP and -rMUA was calculated for each layer by fitting the averaged response with an equation of the form of the Boltzmann charge–voltage function. This equation was solved for its 4th derivative giving a highly accurate measure of the response onset independent of the slope rise phase (Fedchyshyn and Wang 2007). Slopes were measured by using the next equation: $\frac{\Delta V}{t1-t2}$, where ΔV is the LFP amplitude, t_1 is the onset and t_2 is the time of the negative peak.

For analysis of the spontaneous cortical activity, up-states within the slow-wave activity (SWA) were first analysed in periods of 5 minutes of spontaneous HLCx recordings for each subject to compare cortical state immediately before and between 10-30 minutes after SCI. Raw signals were down sampled to 500 Hz and then a Fast Fourier Transform (FFT) analysis was performed to confirm that the maximum peak frequency of the recordings was below 1 Hz. Frequency power (mV^2) was extracted for each electrode by summing power within same frequency band: SWA (0.1-1 Hz), delta (δ, 1-4 Hz), theta (θ, 4-8 Hz), alfa (α, 8-12 Hz), beta (β, 12-25 Hz), low gamma (Lγ, 25-50 Hz) and high gamma (Hγ, 50-80 Hz). LFP power obtained from individual electrodes within a layer was averaged to obtain a layer frequency power. Finally, the power of each frequency band was normalized to the total power of the LFP recording (0.1-80 Hz) to obtain the relative power of each band. Additionally, individual up-states were selected within periods of 60 seconds of LFP for each subject to obtain the onset in control and acute SCI using the same methodology than for the onset of evoked-LFP responses (Fedchyshyn and Wang 2007). To calculate the velocity of propagation, the electrode presenting the earliest onset was taken as reference, and the velocity rate calculated as the distance in the cortical depth as a function of time.

Thalamocortical recordings and analysis

Simultaneous electrophysiological recordings from FLCx and HLCx (n = 7 rats) in response to peripheral forelimb stimulation were obtained by using two single tungsten electrodes located on infragranular layer 5 of both cortical regions under control conditions and after SCI. Note that this dataset was obtained simultaneously to the thalamic data previously published in Alonso-Calviño et al., 2016, but the cortical dataset has been for the first time analysed for the present work. Anaesthesia and stimulation protocol were the same than for experiments explained above. Extracellular recordings were obtained using tungsten electrodes (TM31C40KT, 4-MΩ impedance at 1 kHz or TM31A50KT, 5-MΩ impedance at 1 kHz; World Precision Instruments Inc., Sarasota FL, USA). All recordings were pre-amplified in the DC mode, low pass filtered (<3 kHz) and amplified using a modular system (Neurolog, Digitimer Ltd). Analogue signals were converted into digital data at a 20 kHz with 16–bit quantization via a CED power 1401 apparatus controlled by Spike2 software (v6, Cambridge Electronics Design, Cambridge, UK). The data was analysed using Spike2 software. Onset latency of cortical responses was obtained using the same method than for S1HL multielectrode recordings (Fedchyshyn and Wang 2007) and evoked cortical responses to peripheral forelimb stimulation at 5 mA were used for this analysis.

Histology

At the end of the experiments, animals were transcardially perfused with heparinised saline followed by 4% paraformaldehyde. Then the brain was removed and post-fixed in the same fixative solution for 24h at 4°C. After fixation, brain tissue was cryopreserved in a 30% sucrose solution until sank and coronal sections at 50 µm thick were obtained with a sliding microtome (Microm HM 450 V; Microm International GmbH, Walldorf, Germany). Following washing in 0.1 M phosphate buffer, sections were mounted in gelatin slides, air dried, processed for cresyl violet (Nissl) staining, dehydrated in xylene and coverslipped with DePeX (SEVA Electrophoresis GmbH, Heidelberg, Germany).

Statistical analysis

Animals were randomly assigned to each group. Statistical analyses were performed using Statistica.Ink software (Statsoft Ibérica, Lisboa, Portugal). Grubb´s test was used to detect and eliminate outliers' values in univariate data sets when significance level is $p<0.05$. Control responses (pre lesion) were analysed using a one-way Analysis of Variance (ANOVA), with LAYER as independent factor. Dependent differences between pre- and post-injury among animals and layers were determined by two-way ANOVA, with LAYER as an independent factor and TIME as a repeated measures factor (two levels, PRE- and POST-lesion). When significant differences in ANOVA where found, Tukey´s *post hoc* test was performed. The threshold for statistical significance was $p < 0.05$ throughout. Group measurements are expressed as mean ± standard error of the mean (SEM). Results from statistical analysis are summarized in Table 1-3 of Supplementary material.

SUPPLEMENTARY INFORMATION

See Supplemental Section.

REFERENCES

Aguilar J, Humanes-Valera D, Alonso-Calviño E, Yague JG, Moxon KA, Oliviero A, Foffani G. Spinal cord injury immediately changes the state of the brain. J Neurosci. 2010 Jun 2;30(22):7528-37. doi: 10.1523/JNEUROSCI.0379-10.2010. PMID: 20519527; PMCID: PMC3842476.

Alonso-Calviño E, Martínez-Camero I, Fernández-López E, Humanes-Valera D, Foffani G, Aguilar J. Increased responses in the somatosensory thalamus immediately after spinal cord injury. Neurobiol Dis. 2016 Mar;87:39-49. doi: 10.1016/j.nbd.2015.12.003. Epub 2015 Dec 17. PMID: 26706597.

Barnes SJ, Franzoni E, Jacobsen RI, Erdelyi F, Szabo G, Clopath C, Keller GB, Keck T. Deprivation-Induced Homeostatic Spine Scaling In Vivo Is Localized to Dendritic Branches that Have Undergone Recent Spine Loss. Neuron. 2017 Nov 15;96(4):871-882.e5. doi: 10.1016/j.neuron.2017.09.052. Epub 2017 Nov 5. PMID: 29107520; PMCID: PMC5697914.

Bayraktar OA, Bartels T, Holmqvist S, Kleshchevnikov V, Martirosyan A, Polioudakis D, Ben Haim L, Young AMH, Batiuk MY, Prakash K, Brown A, Roberts K, Paredes MF, Kawaguchi R, Stockley JH, Sabeur K, Chang SM, Huang E, Hutchinson P, Ullian EM, Hemberg M, Coppola G, Holt MG, Geschwind DH, Rowitch DH. Astrocyte layers in the mammalian cerebral cortex revealed by a single-cell in situ transcriptomic map. Nat Neurosci. 2020 Apr;23(4):500-509. doi: 10.1038/s41593-020-0602-1. Epub 2020 Mar 16. PMID: 32203496.

Bola Ł, Zimmermann M, Mostowski P, Jednoróg K, Marchewka A, Rutkowski P, Szwed M. Task-specific reorganization of the auditory cortex in deaf humans. Proc Natl Acad Sci U S A. 2017 Jan 24;114(4):E600-E609. doi: 10.1073/pnas.1609000114. Epub 2017 Jan 9. PMID: 28069964; PMCID: PMC5278486.

Buzsáki G, Anastassiou CA, Koch C. The origin of extracellular fields and currents--EEG, ECoG, LFP and spikes. Nat Rev Neurosci. 2012 May 18;13(6):407-20. doi: 10.1038/nrn3241. PMID: 22595786; PMCID: PMC4907333.

Cardin JA, Carlén M, Meletis K, Knoblich U, Zhang F, Deisseroth K, Tsai LH, Moore CI. Driving fast-spiking cells induces gamma rhythm and controls sensory responses. Nature. 2009 Jun 4;459(7247):663-7. doi: 10.1038/nature08002. Epub 2009 Apr 26. PMID: 19396156; PMCID: PMC3655711.

Castro-Alamancos MA. Cortical up and activated states: implications for sensory information processing. Neuroscientist. 2009 Dec;15(6):625-34. doi: 10.1177/1073858409333074. PMID: 19321459; PMCID: PMC7701994.

Chapin JK, Lin CS. Mapping the body representation in the SI cortex of anesthetized and awake rats. J Comp Neurol. 1984 Oct 20;229(2):199-213. doi: 10.1002/cne.902290206. PMID: 6438190.

Chauvette S, Volgushev M, Timofeev I. Origin of active states in local neocortical networks during slow sleep oscillation. Cereb Cortex. 2010 Nov;20(11):2660-74. doi: 10.1093/cercor/bhq009. Epub 2010 Mar 3. PMID: 20200108; PMCID: PMC2951844.

Compte A, Sanchez-Vives MV, McCormick DA, Wang XJ. Cellular and network mechanisms of slow oscillatory activity (<1 Hz) and wave propagations in a cortical network model. J Neurophysiol. 2003 May;89(5):2707-25. doi: 10.1152/jn.00845.2002. Epub 2003 Jan 15. PMID: 12612051.

Curt A, Bruehlmeier M, Leenders KL, Roelcke U, Dietz V. Differential effect of spinal cord injury and functional impairment on human brain activation. J Neurotrauma. 2002 Jan;19(1):43-51. doi: 10.1089/089771502753460222. PMID: 11852977.

David F, Schmiedt JT, Taylor HL, Orban G, Di Giovanni G, Uebele VN, Renger JJ, Lambert RC, Leresche N, Crunelli V. Essential thalamic contribution to slow waves of natural sleep. J Neurosci. 2013 Dec 11;33(50):19599-610. doi: 10.1523/JNEUROSCI.3169-13.2013. PMID: 24336724; PMCID: PMC3858629.

De Pasquale R, Sherman SM. Synaptic properties of corticocortical connections between the primary and secondary visual cortical areas in the mouse. J Neurosci. 2011 Nov 16;31(46):16494-506. doi: 10.1523/JNEUROSCI.3664-11.2011. PMID: 22090476; PMCID: PMC3233982.

Derdikman D, Yu C, Haidarliu S, Bagdasarian K, Arieli A, Ahissar E. Layer-specific touch-dependent facilitation and depression in the somatosensory cortex during active whisking. J Neurosci. 2006 Sep 13;26(37):9538-47. doi: 10.1523/JNEUROSCI.0918-06.2006. PMID: 16971538; PMCID: PMC6674596.

Dutta A, Kambi N, Raghunathan P, Khushu S, Jain N. Large-scale reorganization of the somatosensory cortex of adult macaque monkeys revealed by fMRI. Brain Struct Funct. 2014 Jul;219(4):1305-20.

doi: 10.1007/s00429-013-0569-8. Epub 2013 May 8. PMID: 23652854.

Endo T, Spenger C, Tominaga T, Brené S, Olson L. Cortical sensory map rearrangement after spinal cord injury: fMRI responses linked to Nogo signalling. Brain. 2007 Nov;130(Pt 11):2951-61. doi: 10.1093/brain/awm237. Epub 2007 Oct 3. PMID: 17913768.

Favero M, Castro-Alamancos MA. Synaptic cooperativity regulates persistent network activity in neocortex. J Neurosci. 2013 Feb 13;33(7):3151-63. doi: 10.1523/JNEUROSCI.4424-12.2013. Erratum in: J Neurosci. 2017 Mar 29;37(13):3734. PMID: 23407969; PMCID: PMC3711603.

Fedchyshyn MJ, Wang LY. Activity-dependent changes in temporal components of neurotransmission at the juvenile mouse calyx of Held synapse. J Physiol. 2007 Jun 1;581(Pt 2):581-602. doi: 10.1113/jphysiol.2007.129833. Epub 2007 Mar 8. PMID: 17347264; PMCID: PMC2075169.

Fernández-López E, Alonso-Calviño E, Humanes-Valera D, Foffani G, Aguilar J. Slow-wave activity homeostasis in the somatosensory cortex after spinal cord injury. Exp Neurol. 2019 Dec;322:113035. doi: 10.1016/j.expneurol.2019.113035. Epub 2019 Aug 22. PMID: 31446080.

Fiáth R, Kerekes BP, Wittner L, Tóth K, Beregszászi P, Horváth D, Ulbert I. Laminar analysis of the slow wave activity in the somatosensory cortex of anesthetized rats. Eur J Neurosci. 2016 Aug;44(3):1935-51. doi: 10.1111/ejn.13274. Epub 2016 Jun 9. PMID: 27177594.

Fiáth R, Márton AL, Mátyás F, Pinke D, Márton G, Tóth K, Ulbert I. Slow insertion of silicon probes improves the quality of acute neuronal recordings. Sci Rep. 2019 Jan 14;9(1):111. doi: 10.1038/s41598-018-36816-z. PMID: 30643182; PMCID: PMC6331571.

Francis JT, Xu S, Chapin JK. Proprioceptive and cutaneous representations in the rat ventral posterolateral thalamus. J Neurophysiol. 2008 May;99(5):2291-304. doi: 10.1152/jn.01206.2007. Epub 2008 Feb 20. PMID: 18287546.

Freund P, Weiskopf N, Ashburner J, Wolf K, Sutter R, Altmann DR, Friston K, Thompson A, Curt A. MRI investigation of the sensorimotor cortex and the corticospinal tract after acute spinal cord injury: a prospective longitudinal study. Lancet Neurol. 2013 Sep;12(9):873-881. doi: 10.1016/S1474-4422(13)70146-7. Epub 2013 Jul 2. Erratum in: Lancet Neurol. 2013 Sep;12(9):846. PMID: 23827394; PMCID: PMC3744750.

Ghosh A, Haiss F, Sydekum E, Schneider R, Gullo M, Wyss MT, Mueggler T, Baltes C, Rudin M, Weber B, Schwab ME. Rewiring of hindlimb corticospinal neurons after spinal cord injury. Nat Neurosci. 2010 Jan;13(1):97-104. doi: 10.1038/nn.2448. Epub 2009 Dec 13. PMID: 20010824.

Green JB, Sora E, Bialy Y, Ricamato A, Thatcher RW. Cortical sensorimotor reorganization after spinal cord injury: an electroencephalographic study. Neurology. 1998 Apr;50(4):1115-21. doi: 10.1212/wnl.50.4.1115. PMID: 9566404.

Griffen TC, Haley MS, Fontanini A, Maffei A. Rapid plasticity of visually evoked responses in rat monocular visual cortex. PLoS One. 2017 Sep 14;12(9):e0184618. doi: 10.1371/journal.pone.0184618. PMID: 28910338; PMCID: PMC5598998.

Gruber T, Tsivilis D, Montaldi D, Müller MM. Induced gamma band responses: an early marker of memory encoding and retrieval. Neuroreport. 2004 Aug 6;15(11):1837-41. doi: 10.1097/01.wnr.0000137077.26010.12. PMID: 15257158.

Gustin SM, Wrigley PJ, Siddall PJ, Henderson LA. Brain anatomy changes associated with persistent neuropathic pain following spinal cord injury. Cereb Cortex. 2010 Jun;20(6):1409-19. doi: 10.1093/cercor/bhp205. Epub 2009 Oct 8. PMID: 19815621.

Han Y, Li N, Zeiler SR, Pelled G. Peripheral nerve injury induces immediate increases in layer v neuronal activity. Neurorehabil Neural Repair. 2013 Sep;27(7):664-72. doi: 10.1177/1545968313484811. Epub 2013 Apr 18. PMID: 23599222; PMCID: PMC3729632.

He HY, Hodos W, Quinlan EM. Visual deprivation reactivates rapid ocular dominance plasticity in adult visual cortex. J Neurosci. 2006 Mar 15;26(11):2951-5. doi: 10.1523/JNEUROSCI.5554-05.2006. PMID: 16540572; PMCID: PMC6673977.

Humanes-Valera D, Aguilar J, Foffani G. Reorganization of the intact somatosensory cortex immediately after spinal cord injury. PLoS One. 2013 Jul 29;8(7):e69655. doi: 10.1371/journal.pone.0069655. PMID: 23922771; PMCID: PMC3726757.

Humanes-Valera D, Foffani G, Alonso-Calviño E, Fernández-López E, Aguilar J. Dual Cortical Plasticity After Spinal Cord Injury. Cereb Cortex.

2017 May 1;27(5):2926-2940. doi: 10.1093/cercor/bhw142. PMID: 27226441.

Jain N, Florence SL, Kaas JH. Reorganization of Somatosensory Cortex After Nerve and Spinal Cord Injury. News Physiol Sci. 1998 Jun;13:143-149. doi: 10.1152/physiologyonline.1998.13.3.143. PMID: 11390778.

Jain N, Florence SL, Qi HX, Kaas JH. Growth of new brainstem connections in adult monkeys with massive sensory loss. Proc Natl Acad Sci U S A. 2000 May 9;97(10):5546-50. doi: 10.1073/pnas.090572597. PMID: 10779564; PMCID: PMC25865.

Jain N, Qi HX, Collins CE, Kaas JH. Large-scale reorganization in the somatosensory cortex and thalamus after sensory loss in macaque monkeys. J Neurosci. 2008 Oct 22;28(43):11042-60. doi: 10.1523/JNEUROSCI.2334-08.2008. PMID: 18945912; PMCID: PMC2613515.

Jutzeler CR, Curt A, Kramer JL. Relationship between chronic pain and brain reorganization after deafferentation: A systematic review of functional MRI findings. Neuroimage Clin. 2015 Oct 3;9:599-606. doi: 10.1016/j.nicl.2015.09.018. PMID: 26740913; PMCID: PMC4644246.

Jutzeler CR, Streijger F, Aguilar J, Shortt K, Manouchehri N, Okon E, Hupp M, Curt A, Kwon BK, Kramer JLK. Sensorimotor plasticity after spinal cord injury: a longitudinal and translational study. Ann Clin Transl Neurol. 2018 Dec 1;6(1):68-82. doi: 10.1002/acn3.679. PMID: 30656185; PMCID: PMC6331953.

Kao T, Shumsky JS, Murray M, Moxon KA. Exercise induces cortical plasticity after neonatal spinal cord injury in the rat. J Neurosci. 2009 Jun 10;29(23):7549-57. doi: 10.1523/JNEUROSCI.2474-08.2009. PMID: 19515923; PMCID: PMC2743445.

Keck T, Keller GB, Jacobsen RI, Eysel UT, Bonhoeffer T, Hübener M. Synaptic scaling and homeostatic plasticity in the mouse visual cortex in vivo. Neuron. 2013 Oct 16;80(2):327-34. doi: 10.1016/j.neuron.2013.08.018. PMID: 24139037.

Kuki T, Fujihara K, Miwa H, Tamamaki N, Yanagawa Y, Mushiake H. Contribution of parvalbumin and somatostatin-expressing GABAergic neurons to slow oscillations and the balance in beta-gamma oscillations across cortical layers. Front Neural Circuits. 2015 Feb 3;9:6. doi: 10.3389/fncir.2015.00006. PMID: 25691859; PMCID: PMC4315041.

Liang L, Mendell LM. Bilateral transient changes in thalamic nucleus ventroposterior lateralis after thoracic hemisection in the rat. J Neurophysiol. 2013 Aug;110(4):942-51. doi: 10.1152/jn.00998.2012. Epub 2013 Jun 5. PMID: 23741041; PMCID: PMC3742973.

Lilja J, Endo T, Hofstetter C, Westman E, Young J, Olson L, Spenger C. Blood oxygenation level-dependent visualization of synaptic relay stations of sensory pathways along the neuroaxis in response to graded sensory stimulation of a limb. J Neurosci. 2006 Jun 7;26(23):6330-6. doi: 10.1523/JNEUROSCI.0626-06.2006. PMID: 16763041; PMCID: PMC6675206.

Makin TR, Scholz J, Filippini N, Henderson Slater D, Tracey I, Johansen-Berg H. Phantom pain is associated with preserved structure and function in the former hand area. Nat Commun. 2013;4:1570. doi: 10.1038/ncomms2571. PMID: 23463013; PMCID: PMC3615341.

Minlebaev M, Colonnese M, Tsintsadze T, Sirota A, Khazipov R. Early γ oscillations synchronize developing thalamus and cortex. Science. 2011 Oct 14;334(6053):226-9. doi: 10.1126/science.1210574. PMID: 21998388.

Morales-Botello ML, Aguilar J, Foffani G. Imaging the spatio-temporal dynamics of supragranular activity in the rat somatosensory cortex in response to stimulation of the paws. PLoS One. 2012;7(7):e40174. doi: 10.1371/journal.pone.0040174. Epub 2012 Jul 19. PMID: 22829873; PMCID: PMC3400596.

Moxon KA, Hale LL, Aguilar J, Foffani G. Responses of infragranular neurons in the rat primary somatosensory cortex to forepaw and hindpaw tactile stimuli. Neuroscience. 2008 Oct 28;156(4):1083-92. doi: 10.1016/j.neuroscience.2008.08.009. Epub 2008 Aug 12. PMID: 18775766.

Moxon KA, Oliviero A, Aguilar J, Foffani G. Cortical reorganization after spinal cord injury: always for good? Neuroscience. 2014 Dec 26;283:78-94. doi: 10.1016/j.neuroscience.2014.06.056. Epub 2014 Jul 2. PMID: 24997269; PMCID: PMC4556279.

Muret D, Makin TR. The homeostatic homunculus: rethinking deprivation-triggered reorganisation. Curr Opin Neurobiol. 2020 Nov 25;67:115-122. doi: 10.1016/j.conb.2020.08.008. Epub ahead of print. PMID: 33248404.

Ortmann M, Müller N, Schlee W, Weisz N. Rapid increases of gamma power in the auditory cortex following noise trauma in humans. Eur J Neurosci. 2011 Feb;33(3):568-75. doi: 10.1111/j.1460-

9568.2010.07542.x. Epub 2010 Dec 29. PMID: 21198988.

Paxinos G, Watson C. The rat brain in stereotaxic coordinates. Amsterdam: Academic Press. 2007.

Peyron R, Schneider F, Faillenot I, Convers P, Barral FG, Garcia-Larrea L, Laurent B. An fMRI study of cortical representation of mechanical allodynia in patients with neuropathic pain. Neurology. 2004 Nov 23;63(10):1838-46. doi: 10.1212/01.wnl.0000144177.61125.85. PMID: 15557499.

Puig MV, Ushimaru M, Kawaguchi Y. Two distinct activity patterns of fast-spiking interneurons during neocortical UP states. Proc Natl Acad Sci U S A. 2008 Jun 17;105(24):8428-33. doi: 10.1073/pnas.0712219105. Epub 2008 Jun 12. PMID: 18550841; PMCID: PMC2448853.

Rigas P, Castro-Alamancos MA. Impact of persistent cortical activity (up States) on intracortical and thalamocortical synaptic inputs. J Neurophysiol. 2009 Jul;102(1):119-31. doi: 10.1152/jn.00126.2009. Epub 2009 Apr 29. PMID: 19403750; PMCID: PMC2712261.

Rossignol S, Frigon A. Recovery of locomotion after spinal cord injury: some facts and mechanisms. Annu Rev Neurosci. 2011; 34:413-40. doi: 10.1146/annurev-neuro-061010-113746. PMID: 21469957.

Sakata S, Harris KD. Laminar structure of spontaneous and sensory-evoked population activity in auditory cortex. Neuron. 2009 Nov 12;64(3):404-18. doi: 10.1016/j.neuron.2009.09.020. PMID: 19914188; PMCID: PMC2778614.

Sanchez-Vives MV, McCormick DA. Cellular and network mechanisms of rhythmic recurrent activity in neocortex. Nat Neurosci. 2000 Oct;3(10):1027-34. doi: 10.1038/79848. PMID: 11017176.

Schoffelen JM, Poort J, Oostenveld R, Fries P. Selective movement preparation is subserved by selective increases in corticomuscular gamma-band coherence. J Neurosci. 2011 May 4;31(18):6750-8. doi: 10.1523/JNEUROSCI.4882-10.2011. PMID: 21543604; PMCID: PMC6632864.

Schroeder CE, Mehta AD, Givre SJ. A spatiotemporal profile of visual system activation revealed by current source density analysis in the awake macaque. Cereb Cortex. 1998 Oct-Nov;8(7):575-92. doi: 10.1093/cercor/8.7.575. PMID: 9823479.

Schubert D, Kötter R, Staiger JF. Mapping functional connectivity in barrel-related columns reveals layer- and cell type-specific microcircuits. Brain Struct Funct. 2007 Sep;212(2):107-19. doi: 10.1007/s00429-007-0147-z. Epub 2007 Jun 26. PMID: 17717691.

Siddall PJ, Loeser JD. Pain following spinal cord injury. Spinal Cord. 2001 Feb;39(2):63-73. doi: 10.1038/sj.sc.3101116. PMID: 11402361.

Siddall PJ, McClelland JM, Rutkowski SB, Cousins MJ. A longitudinal study of the prevalence and characteristics of pain in the first 5 years following spinal cord injury. Pain. 2003 Jun;103(3):249-57. doi: 10.1016/s0304-3959(02)00452-9. PMID: 12791431.

Steriade M, McCormick DA, Sejnowski TJ. Thalamocortical oscillations in the sleeping and aroused brain. Science. 1993 Oct 29;262(5134):679-85. doi: 10.1126/science.8235588. PMID: 8235588.

Sydekum E, Ghosh A, Gullo M, Baltes C, Schwab M, Rudin M. Rapid functional reorganization of the forelimb cortical representation after thoracic spinal cord injury in adult rats. Neuroimage. 2014 Feb 15;87:72-9. doi: 10.1016/j.neuroimage.2013.10.045. Epub 2013 Oct 31. PMID: 24185021.

Tan LL, Oswald MJ, Heinl C, Retana Romero OA, Kaushalya SK, Monyer H, Kuner R. Gamma oscillations in somatosensory cortex recruit prefrontal and descending serotonergic pathways in aversion and nociception. Nat Commun. 2019 Feb 28;10(1):983. doi: 10.1038/s41467-019-08873-z. PMID: 30816113; PMCID: PMC6395755.

Teichert M, Liebmann L, Hübner CA, Bolz J. Homeostatic plasticity and synaptic scaling in the adult mouse auditory cortex. Sci Rep. 2017 Dec 12;7(1):17423. doi: 10.1038/s41598-017-17711-5. PMID: 29234064; PMCID: PMC5727212.

Timofeev I, Grenier F, Bazhenov M, Sejnowski TJ, Steriade M. Origin of slow cortical oscillations in deafferented cortical slabs. Cereb Cortex. 2000 Dec;10(12):1185-99. doi: 10.1093/cercor/10.12.1185. PMID: 11073868.

Veit J, Hakim R, Jadi MP, Sejnowski TJ, Adesnik H. Cortical gamma band synchronization through somatostatin interneurons. Nat Neurosci. 2017 Jul;20(7):951-959. doi: 10.1038/nn.4562. Epub 2017 May 8. PMID: 28481348; PMCID: PMC5511041.

Welle CG, Contreras D. Sensory-driven and spontaneous gamma oscillations engage distinct cortical circuitry. J Neurophysiol. 2016 Apr;115(4):1821-35. doi: 10.1152/jn.00137.2015.

Epub 2015 Dec 30. PMID: 26719085; PMCID: PMC4869477.

Wester JC, Contreras D. Columnar interactions determine horizontal propagation of recurrent network activity in neocortex. J Neurosci. 2012 Apr 18;32(16):5454-71. doi: 10.1523/JNEUROSCI.5006-11.2012. PMID: 22514308; PMCID: PMC3415278.

Wester JC, Contreras D. Differential modulation of spontaneous and evoked thalamocortical network activity by acetylcholine level in vitro. J Neurosci. 2013 Nov 6;33(45):17951-66. doi: 10.1523/JNEUROSCI.1644-13.2013. PMID: 24198382; PMCID: PMC3818561.

Wilent WB, Contreras D. Synaptic responses to whisker deflections in rat barrel cortex as a function of cortical layer and stimulus intensity. J Neurosci. 2004 Apr 21;24(16):3985-98. doi: 10.1523/JNEUROSCI.5782-03.2004. PMID: 15102914; PMCID: PMC6729426.

Wrigley PJ, Press SR, Gustin SM, Macefield VG, Gandevia SC, Cousins MJ, Middleton JW, Henderson LA, Siddall PJ. Neuropathic pain and primary somatosensory cortex reorganization following spinal cord injury. Pain. 2009 Jan;141(1-2):52-9. doi: 10.1016/j.pain.2008.10.007. Epub 2008 Nov 21. PMID: 19027233.

Yague JG, Foffani G, Aguilar J. Cortical hyperexcitability in response to preserved spinothalamic inputs immediately after spinal cord hemisection. Exp Neurol. 2011 Feb;227(2):252-63. doi: 10.1016/j.expneurol.2010.11.011. Epub 2010 Nov 17. PMID: 21093438.

Yagüe JG, Humanes-Valera D, Aguilar J, Foffani G. Functional reorganization of the forepaw cortical representation immediately after thoracic spinal cord hemisection in rats. Exp Neurol. 2014 Jul;257:19-24. doi: 10.1016/j.expneurol.2014.03.015. Epub 2014 Mar 28. PMID: 24685666.

Yamashita T, Vavladeli A, Pala A, Galan K, Crochet S, Petersen SSA, Petersen CCH. Diverse Long-Range Axonal Projections of Excitatory Layer 2/3 Neurons in Mouse Barrel Cortex. Front Neuroanat. 2018 May 1;12:33. doi: 10.3389/fnana.2018.00033. PMID: 29765308; PMCID: PMC5938399.

FIGURE TITLES AND LEGENDS

Figure 1: Experimental approach and laminar characterization of evoked sensory responses in hindlimb cortex. (A) Schematic illustration of the experimental protocol. Extracellular recordings were obtained using a multielectrode probe inserted in the hindlimb representation of the primary somatosensory cortex (HLCx) from anaesthetized rats. Complete transection of the spinal cord was performed at thoracic level (SCI, T9-T10). Spontaneous activity (Spont) and evoked responses to electrical stimulation at high (5 mA) and low (0.5 mA) intensity delivered to the contralateral hindlimb (HL stim) and forelimb (FL stim) were recorded following the described timeline in control conditions and immediately after SCI. In the cortical representation, black arrows indicate corticocortical connections and thalamic inputs into FL cortex in response to forepaw stimulation (FL stim). Cortical layers were designated as L2/3, L4, L5 and L6. Dashed black lines indicate boundaries of cortical layers. Corpus callosum, cc; Lateral ventricle, LV; Thalamus, Th. (B) Nissl-stained coronal section of a representative rat showing an electrode track in HL cortex. (C) Left: representative sensory evoked-LFP across HL cortical layers in response to a 5 mA electrical stimulation of the contralateral hindlimb (HL). Recordings obtained on every 100 µm are shown on top of the current source density (CSD) map from the same recordings. Right: averaged evoked-LFP amplitudes as a function of cortical depth in response to low (0.5 mA, grey) and high (5 mA, black) sensory stimulation. (D) Left: High-filtered LFP traces from the same recordings in C showing evoked-MUA signal. Right: Averaged area of rMUA from the same population in C. (E) Left: Representative traces of evoked-LFP overlapped on the CSD map in response to 5 mA forelimb stimulation from the same animal as C-D. Note that in this case current sinks are stronger in L2/3 and L5. Right: averaged evoked-LFP amplitudes as a function of cortical depth in response to low (0.5 mA, grey) and high (5 mA, black) sensory stimulation. (F) Left: High-filtered LFP traces from the same recordings in E showing evoked-MUA signal. Right: Averaged area of rMUA from the same population in E. Dashed black lines indicate borders between layers. Data are mean ± sem (n= 24 rats).

Figure 2: Spinal cord injury induces functional changes in the S1 deprived cortex in a layer-dependent manner. (A) Scheme of an SCI animal showing the place of cortical recordings (HLCx rec) and hindlimb stimulation (HL stim). Examples of averaged evoked-LFP recorded in HLCx in response to HL stim (5 mA). Traces are averaged LFP responses across electrode sites within each layer in control (black) and after SCI (grey). Note that complete spinal cord transection was confirmed by absence of evoked-LFP in HLCx. (B) Examples of averaged evoked-LFP recorded in HLCx in response to forelimb stimulation (FL stim; 5 mA) before (black) and after SCI (grey) in group 1 and group 2 animals. Note the increased evoked-LFP response post SCI in Group 1. (C) Population average of the evoked-LFP amplitude from all animals across layers before (black) and after (grey) SCI. (D) Population average of the evoked-LFP amplitude from the same data in C but separated in Group 1 and Group 2. (E) Original traces of averaged evoked-LFP in control condition (pre, black) and after SCI (grey) showing the time points for slope analysis. (F) Slope of evoked-LFP pre- and post-SCI in Group 1 and Group 2. (G) Time-to-peak of the evoked-LFP responses before and after SCI from t_0 to t_2. Data are mean ± sem (n = 24 rats). Statistical significance is shown by asterisks for SCI effect and lines with asterisks for layer effect in each condition, * $p < 0.05$, ** $p < 0.01$, *** $p < 0.001$. Dots represent individual experiments. See also Figure S1 and S2.

Figure 3: Multi-unity activity in infragranular layers of the HL cortex is increased following SCI. (A) Schematic representation of the experiment and extracellular recordings. LFP (top), multi-unit activity (MUA, middle) and rectified MUA (bottom) in HLCx obtained following forelimb stimulation. (B) Laminar profile of evoked-rMUA as high-filtered recording (black traces) overlapped to a colour map showing averaged HLCx responses to forelimb stimulation at 5 mA from the same animal pre- and post-SCI. Electrodes are 100 µm spaced. (C-D) Averaged evoked-rMUA across electrodes within the same layer pre- and post-SCI from the same representative animal in B and population averaged rMUA area from Group 1 animals. (E-F) Averaged evoked-rMUA across electrodes within the same layer pre- and post-SCI from a representative animal in Group 2 and population averaged rMUA area from Group 2 animals. Data are mean ± sem (n = 13 rats in Group 1, n = 3 rats in Group 2. Statistical significance is shown by asterisks for SCI effect and lines with asterisks for layer effect in each condition, * $p < 0.05$, ** $p < 0.01$, *** $p < 0.001$.

Figure 4: Deprived infragranular layers exhibits delayed evoked-onset responses. (A) Left: onset profile of evoked-LFP in HLCx in response to hindlimb stimulation (HL stim) before SCI. Red markers indicate electrodes in which evoked response started. Grey area indicates the period of response onset taken to highlighted LFP traces (in black) in the right. (B) Latency-onset averaged profile to hindlimb stimulation (5

mA) at left. Note the onset in the thalamorecipient granular layers (L4). Right top: bar graph of the evoked-LFP onset responses. Right bottom: normalized histogram of the evoked-LFP onset probability from. Data used in B contain a representative population (n = 5). (C) Left: onset profiles from the same animal pre- and post-SCI showing averaged evoked-LFP in HLCx in response to forelimb stimulation represented as in A. Middle: colour maps from the same traces that at left laminar profile. White arrows indicate the onset response in L2/3 and L6. Right: Highlighted LFP traces represented as black traces in C. In D-E, latency-onset of the laminar profile (at left) and averaged across layers (at right) by forelimb stimulation (5 mA) is represented for Group 1 for evoked-LFP (D) and -rMUA (E) analysis. Response latency-onset was quantified as the response beginning time (top bar graph) and normalized onset probability (bottom bar graph). Dots represent individual experiments. Data are mean ± sem (n = 19 rats for evoked-LFP and n = 13 rats for evoked-rMUA). Statistical significance is shown by asterisks for SCI effect and lines with asterisks for layer effect in each condition, ** $p < 0.01$, *** $p < 0.001$. See also Figure S2.

Figure 5: Thalamocortical responses in HL cortex are delayed after SCI. (A) Scheme showing the thalamocortical pathways activated after forelimb and hindlimb stimulation. Extracellular recordings were simultaneously obtained from L5 of HLCx (rec) and FLCx (rec) while forelimb stimulation at 5 mA was applied. Colored arrows in thalamic nucleus represent the collaterals allowing reciprocal activation of neighbor regions. (B) Original field potential traces obtained from simultaneous recordings from HLCx (pink traces) and FLCx (green traces) before and after SCI. (C) Averaged bar graphs displaying onset latencies of evoked responses in HLCx and FLCx. Data are mean ± sem (n = 7 rats). Statistical analysis performed by using t-test with Bonferroni correction, * $p < 0.05$.

Figure 6: Onset and propagation of spontaneous up-states is altered after SCI. (A) Example SWA across electrodes (left) showing insets of the sigmoid fitting used to calculate the onset latency (right). Colours indicate distinct layers. (B) Left: Histogram of onset probability across layers of spontaneous up-states pre- and post-SCI. Right: Lines graphs showing percentage of up-states with origin in layer 2/3 or layer 5/6 pre- and post-SCI (mean and individual dispersion). (C) Representative example of spontaneous up-state with origin in layer 2/3. (D) Laminar profile and averaged onset latencies of up-states originating in layer 2/3. (E) Representative example of spontaneous up-state with origin in layer 5. (F) Laminar profile and averaged onset latencies of up-states originating in layer 5/6. Data are mean ± sem (n = 19 rats). * $p < 0.05$, ** $p < 0.01$.

Figure 7: SCI increases high-gamma frequency oscillations in supragranular layers. (A) Example of spontaneous slow wave activity (SWA) profile recorded from HLCx in control conditions. Red traces represent a representative electrode within each cortical layer used for B-C. (B) Color plots showing spontaneous SWA spectrogram in L2/3, L4 and L5/6 pre- and post-SCI. (C) Wideband signal (black) and gamma-filtered (25-80 Hz, gray) traces of SWA from L2/3 and L5/6 with expanded traces of the indicated time window. (D) SWA and gamma relative power from distinct layers before and after SCI. Data are mean ± sem (n = 19 rats). ** $p < 0.01$.

FIGURE 1

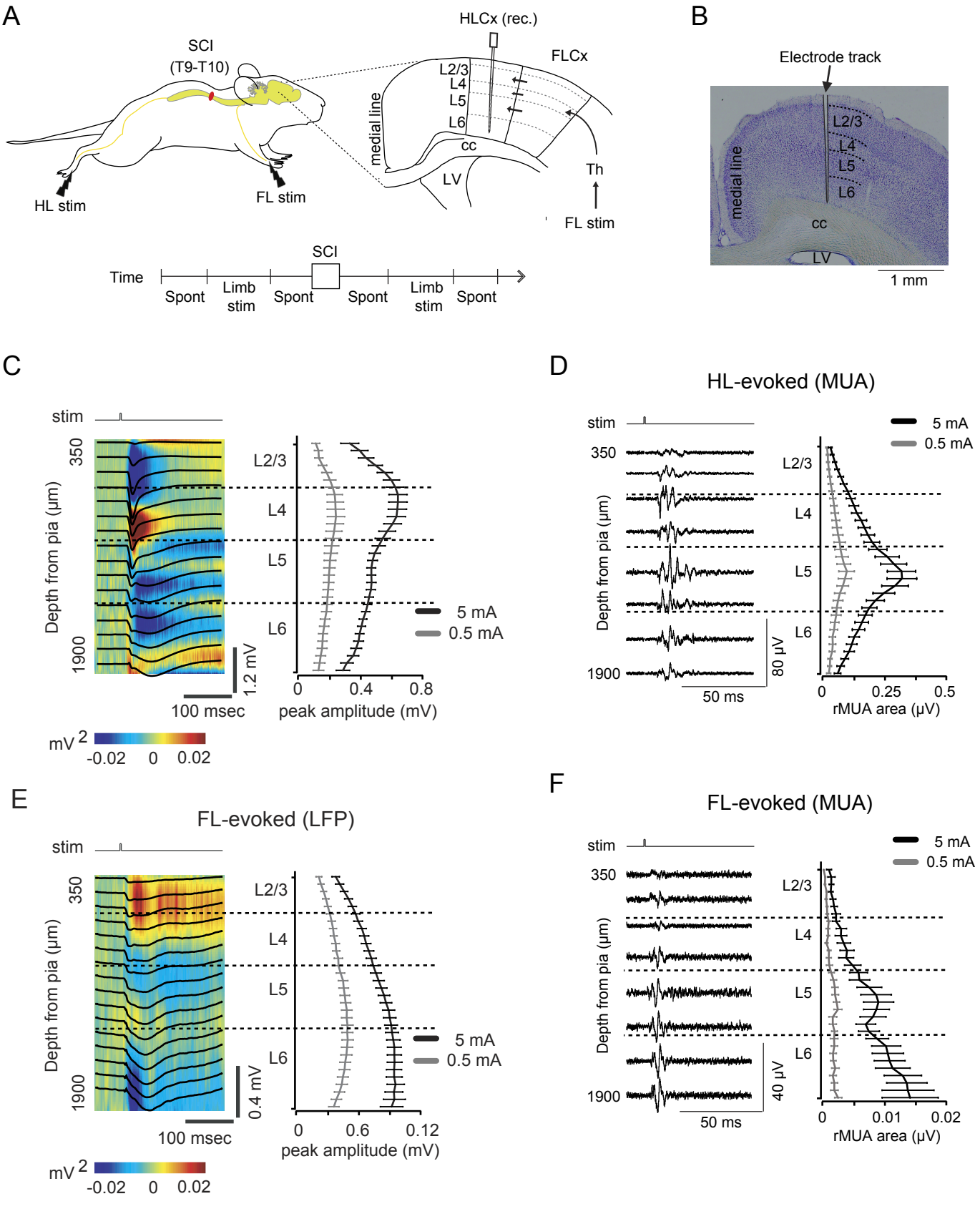
A
SCI
(T9-T10)
HLCx (rec.)
FLCx
L2/3
L4
L5
L6
medial line
cc
LV
Th
HL stim
FL stim
FL stim
Time
SCI
Spont
Limb stim
Spont
Spont
Limb stim
Spont
B
Electrode track
L2/3
L4
L5
L6
medial line
cc
LV
1 mm
C
stim
350
1900
Depth from pia (µm)
L2/3
L4
L5
L6
1.2 mV
100 msec
0
0.4
0.8
peak amplitude (mV)
5 mA
0.5 mA
mV 2
-0.02
0
0.02
D
HL-evoked (MUA)
stim
350
1900
Depth from pia (µm)
5 mA
0.5 mA
L2/3
L4
L5
L6
80 µV
50 ms
0
0.25
0.5
rMUA area (µV)
E
FL-evoked (LFP)
stim
350
1900
Depth from pia (µm)
L2/3
L4
L5
L6
0.4 mV
100 msec
0
0.6
0.12
peak amplitude (mV)
5 mA
0.5 mA
mV 2
-0.02
0
0.02
F
FL-evoked (MUA)
stim
350
1900
Depth from pia (µm)
5 mA
0.5 mA
L2/3
L4
L5
L6
40 µV
50 ms
0
0.01
0.02
rMUA area (µV)

FIGURE 2

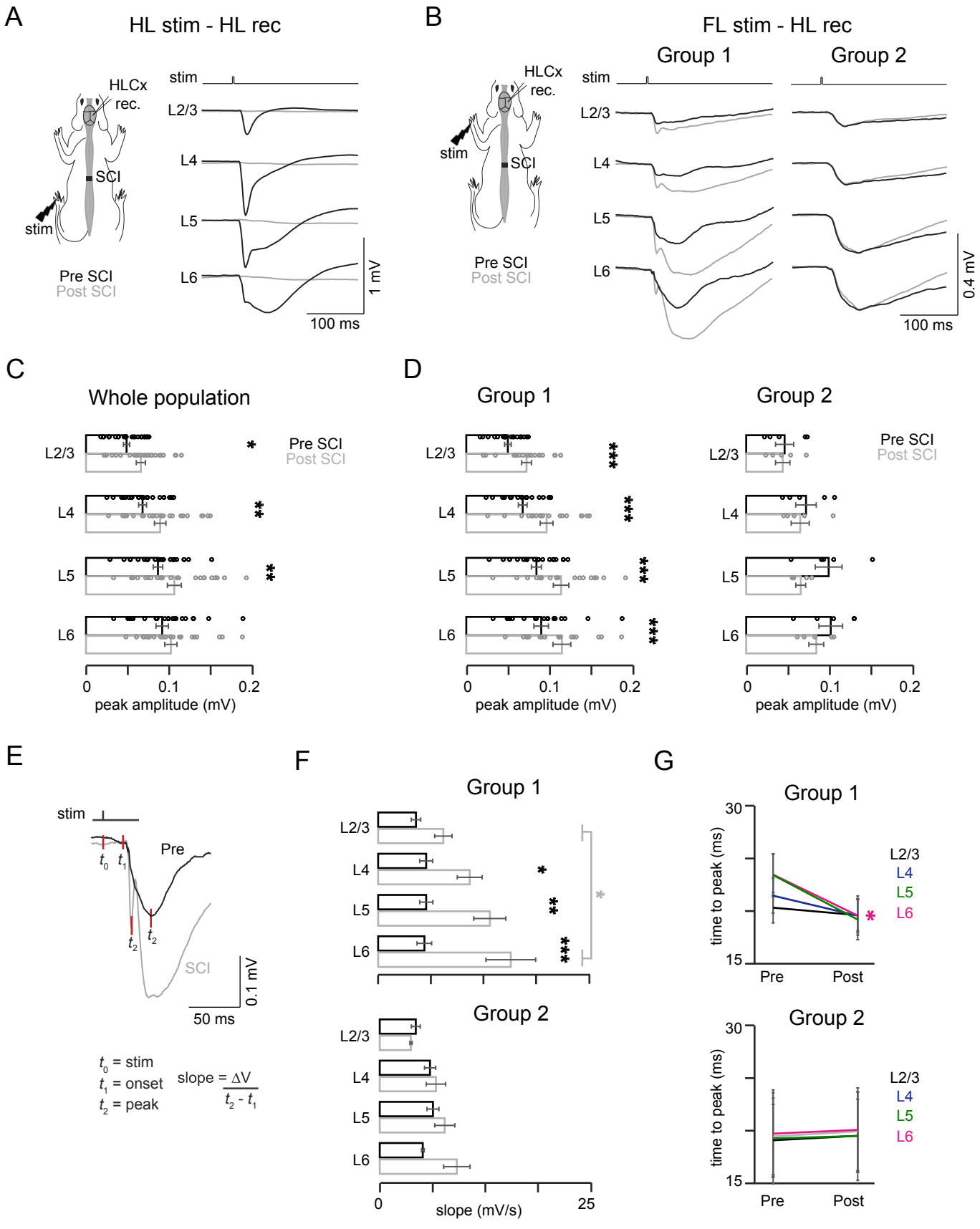
A
HL stim - HL rec
HLCx rec.
SCI
stim
Pre SCI
Post SCI
stim
L2/3
L4
L5
L6
1 mV
100 ms
B
FL stim - HL rec
Group 1
Group 2
HLCx rec.
stim
SCI
Pre SCI
Post SCI
stim
L2/3
L4
L5
L6
0.4 mV
100 ms
C
Whole population
L2/3
L4
L5
L6
Pre SCI
Post SCI
0
0.1
0.2
peak amplitude (mV)
D
Group 1
Group 2
L2/3
L4
L5
L6
Pre SCI
Post SCI
0
0.1
0.2
peak amplitude (mV)
E
stim
Pre
SCI
0.1 mV
50 ms
t_0 = stim
t_1 = onset
t_2 = peak
slope = $\frac{\Delta V}{t_2 - t_1}$
F
Group 1
L2/3
L4
L5
L6
Group 2
L2/3
L4
L5
L6
0
slope (mV/s)
25
G
Group 1
30
15
time to peak (ms)
Pre
Post
L2/3
L4
L5
L6
Group 2
30
15
time to peak (ms)
Pre
Post
L2/3
L4
L5
L6

FIGURE 3

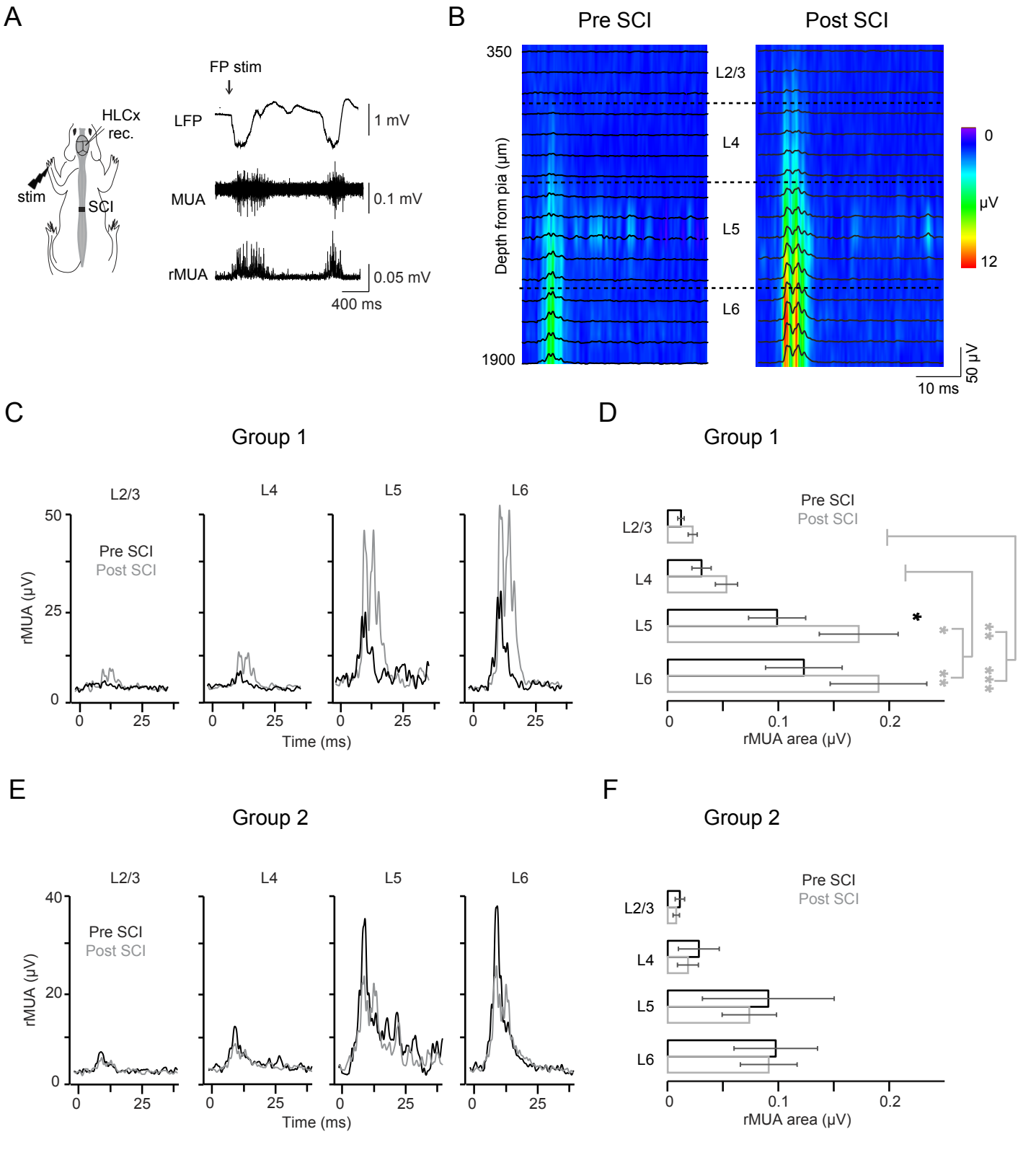
A
HLCx rec.
stim
SCI
FP stim
LFP
1 mV
MUA
0.1 mV
rMUA
0.05 mV
400 ms
B
Pre SCI
Post SCI
350
1900
Depth from pia (µm)
L2/3
L4
L5
L6
0
µV
12
50 µV
10 ms
C
Group 1
L2/3
L4
L5
L6
Pre SCI
Post SCI
rMUA (µV)
Time (ms)
D
Group 1
Pre SCI
Post SCI
rMUA area (µV)
E
Group 2
F
Group 2

FIGURE 4

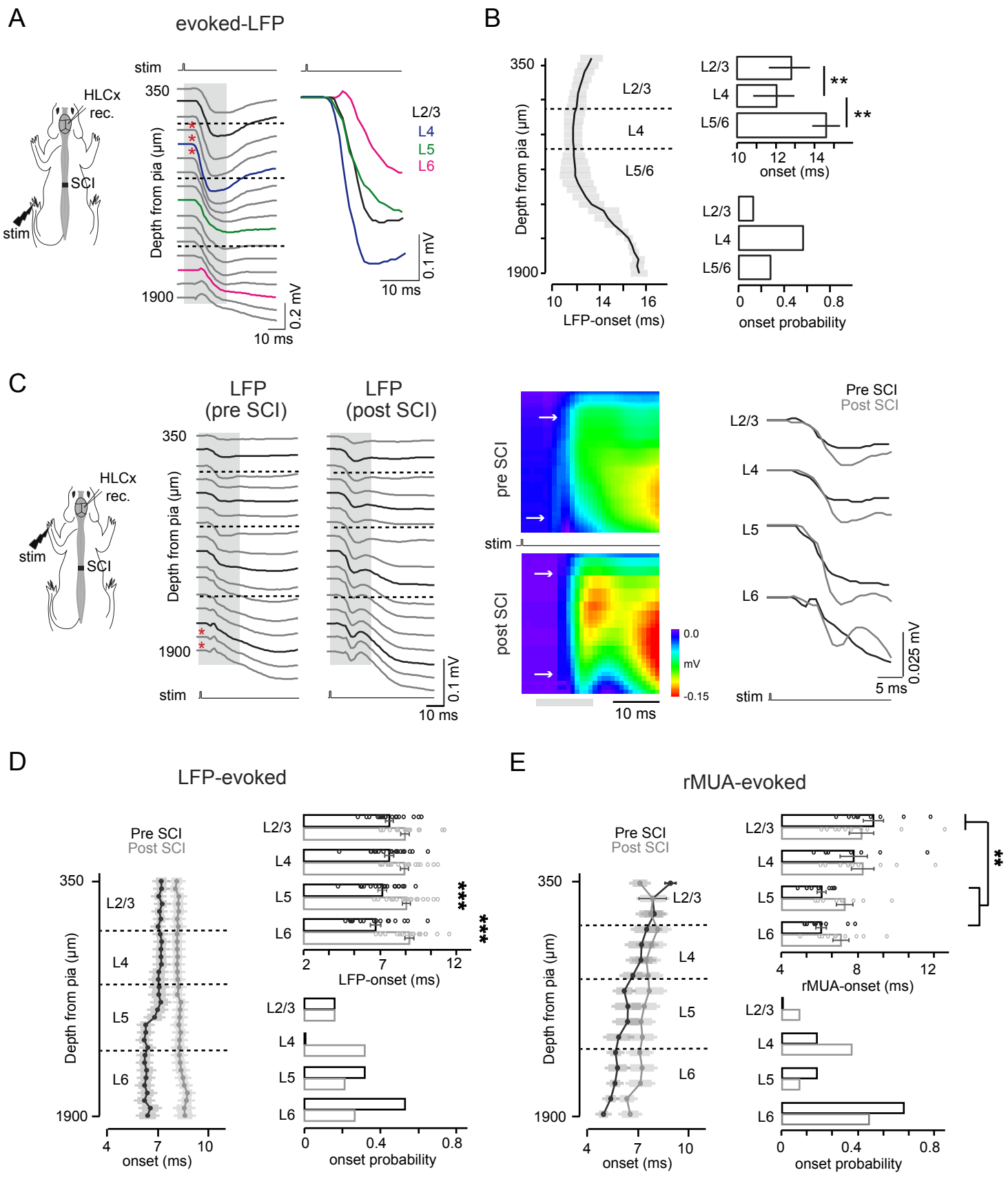
A
evoked-LFP
HLCx
rec.
SCI
stim
Depth from pia (µm)
350
1900
0.2 mV
10 ms
L2/3
L4
L5
L6
0.1 mV
10 ms
B
Depth from pia (µm)
LFP-onset (ms)
onset (ms)
onset probability
**
**
C
LFP
(pre SCI)
LFP
(post SCI)
pre SCI
post SCI
0.0
mV
-0.15
Pre SCI
Post SCI
0.025 mV
5 ms
D
LFP-evoked
Pre SCI
Post SCI
LFP-onset (ms)
onset (ms)
onset probability
***
***
E
rMUA-evoked
rMUA-onset (ms)
**

FIGURE 5

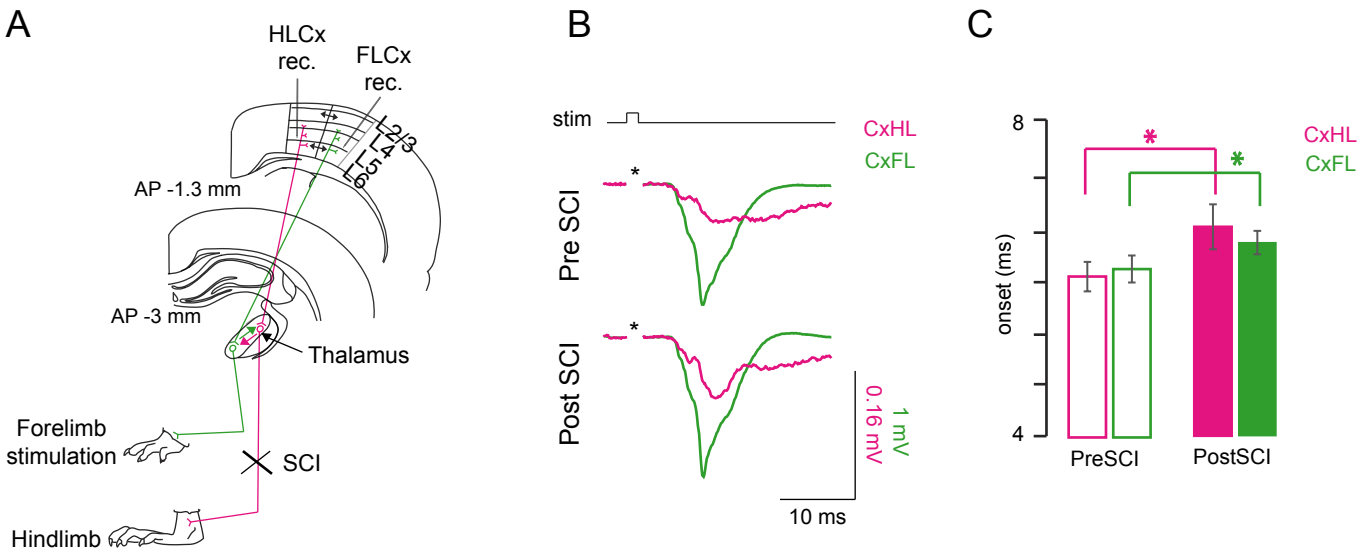
A
HLCx rec.
FLCx rec.
L2/3
L4
L5
AP -1.3 mm
AP -3 mm
Thalamus
Forelimb stimulation
SCI
Hindlimb
B
stim
CxHL
CxFL
Pre SCI
Post SCI
1 mV
0.16 mV
10 ms
C
CxHL
CxFL
onset (ms)
8
4
PreSCI
PostSCI

FIGURE 6

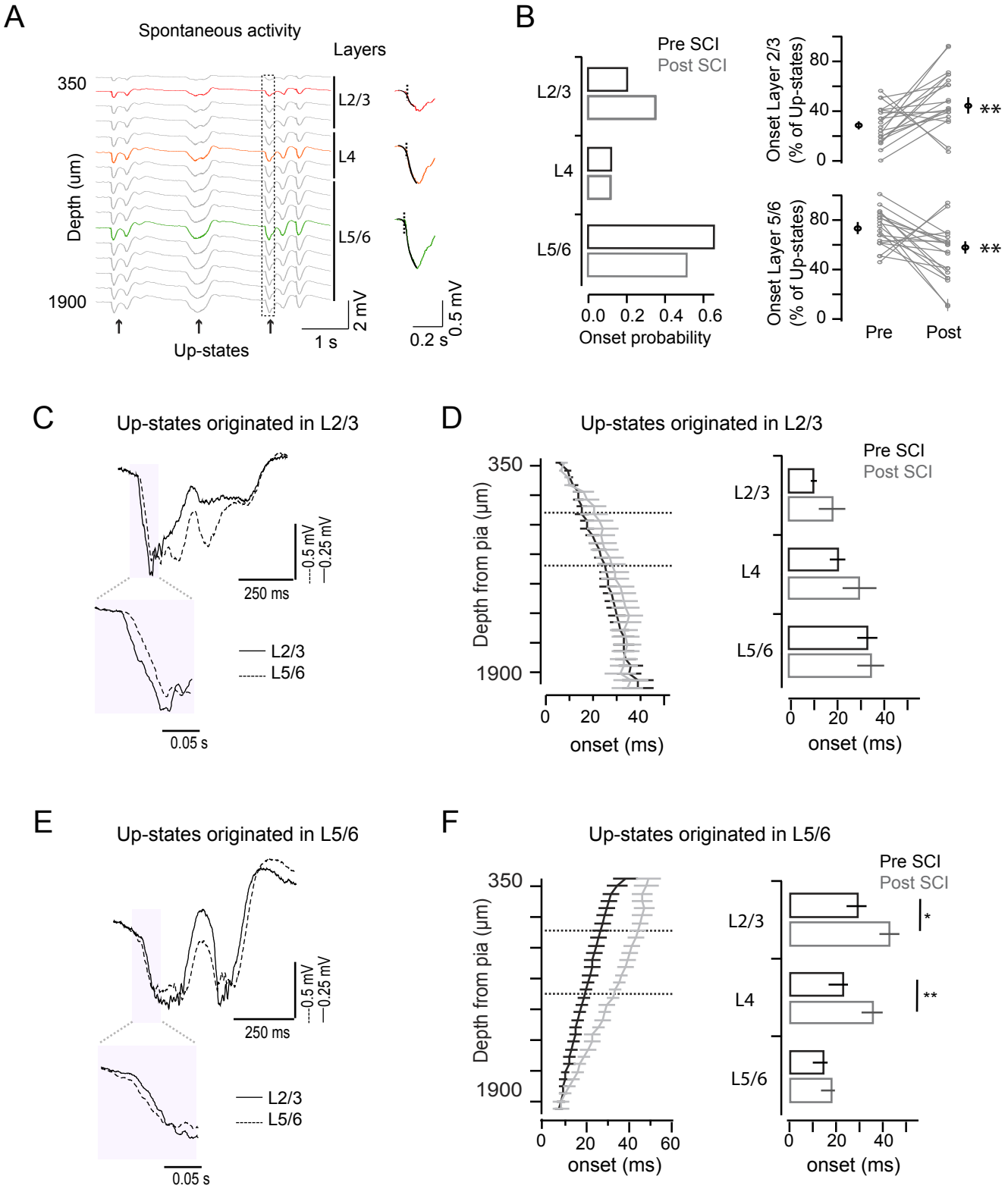
A
Spontaneous activity
Layers
350
Depth (um)
1900
L2/3
L4
L5/6
2 mV
1 s
0.5 mV
0.2 s
Up-states
B
Pre SCI
Post SCI
L2/3
L4
L5/6
0.0 0.2 0.4 0.6
Onset probability
Onset Layer 2/3 (% of Up-states)
Onset Layer 5/6 (% of Up-states)
80
40
0
**
**
Pre
Post
C
Up-states originated in L2/3
0.5 mV
0.25 mV
250 ms
L2/3
L5/6
0.05 s
D
Up-states originated in L2/3
Depth from pia (µm)
350
1900
0 20 40
onset (ms)
Pre SCI
Post SCI
L2/3
L4
L5/6
0 20 40
onset (ms)
E
Up-states originated in L5/6
0.5 mV
0.25 mV
250 ms
L2/3
L5/6
0.05 s
F
Up-states originated in L5/6
Depth from pia (µm)
350
1900
0 20 40 60
onset (ms)
Pre SCI
Post SCI
L2/3
L4
L5/6
*
**
0 20 40
onset (ms)

FIGURE 7

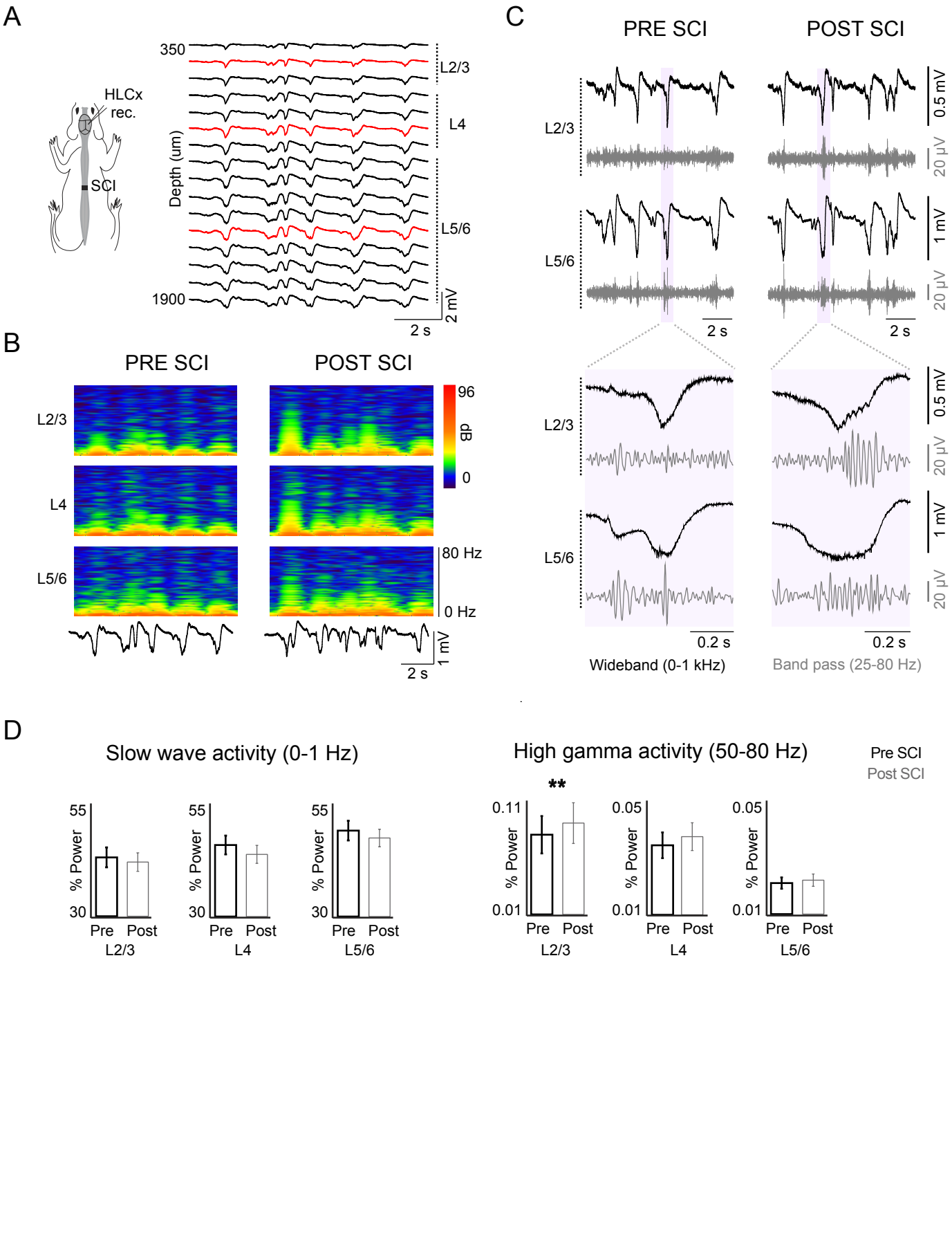
A
HLCx rec.
SCI
350
1900
Depth (um)
L2/3
L4
L5/6
2 mV
2 s
B
PRE SCI
POST SCI
L2/3
L4
L5/6
96
dB
0
80 Hz
0 Hz
1 mV
2 s
C
PRE SCI
POST SCI
L2/3
L5/6
0.5 mV
20 µV
1 mV
20 µV
2 s
0.2 s
Wideband (0-1 kHz)
Band pass (25-80 Hz)
D
Slow wave activity (0-1 Hz)
High gamma activity (50-80 Hz)
Pre SCI
Post SCI
**
% Power
55
30
0.11
0.01
0.05
0.01
Pre
Post
L2/3
L4
L5/6

Supplemental Figure 1

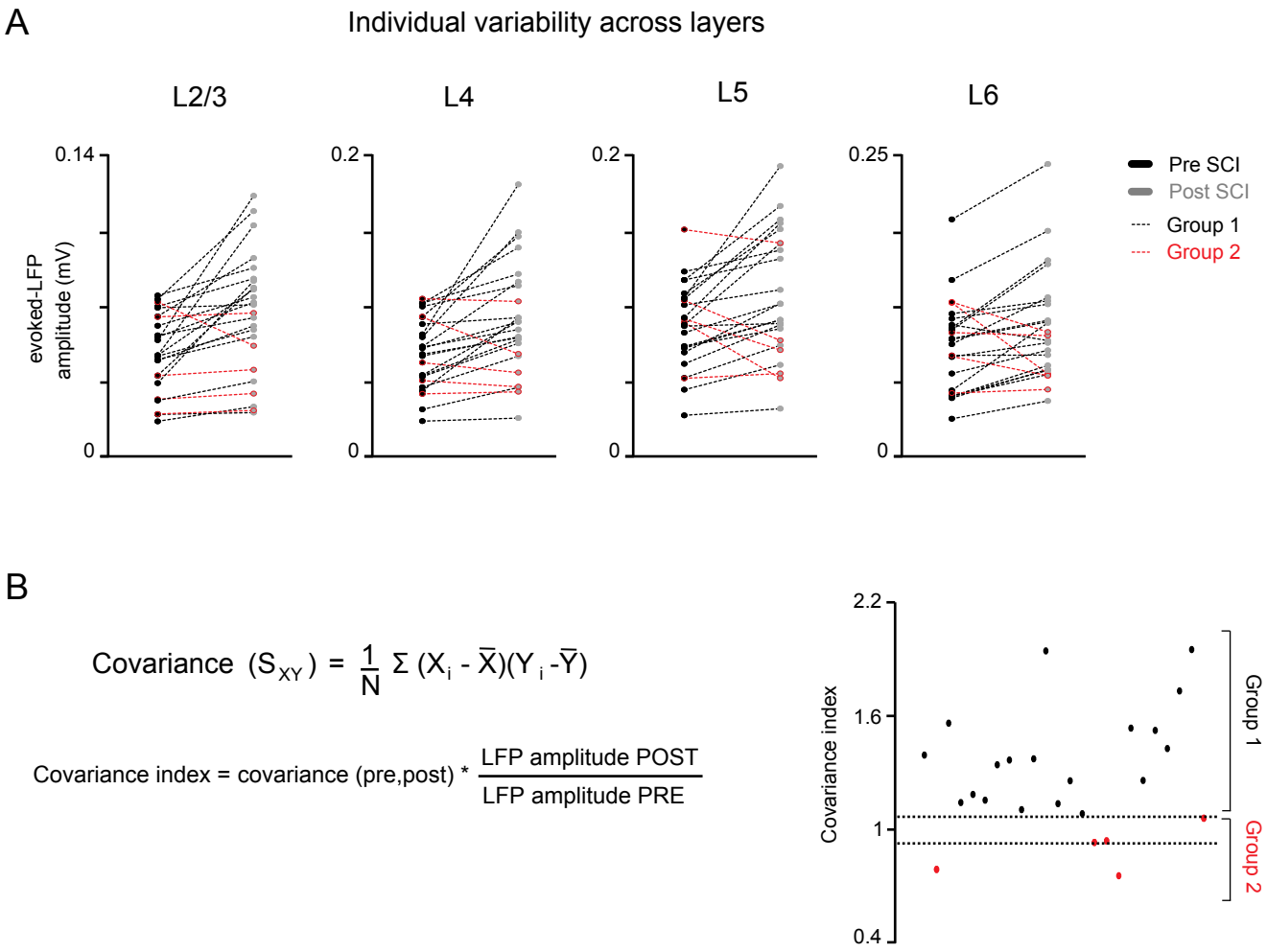

Supplemental Figure 1: Related to Figure 2, Individual variability on LFP responses induced by SCI. (A) Individual evoked-LFP responses in pre- and post-SCI from all individuals in each layer of the HL cortex. Dots represent individual values (black is Group 1 and red is Group 2). (B) Covariance index analysis of the effects of SCI in the amplitude of evoked-LFP. This analysis was used to define individual within Group 1 and Group 2. Dotted line represents the coefficient interval boundaries of this analysis used to group the population.

Supplemental Figure 2

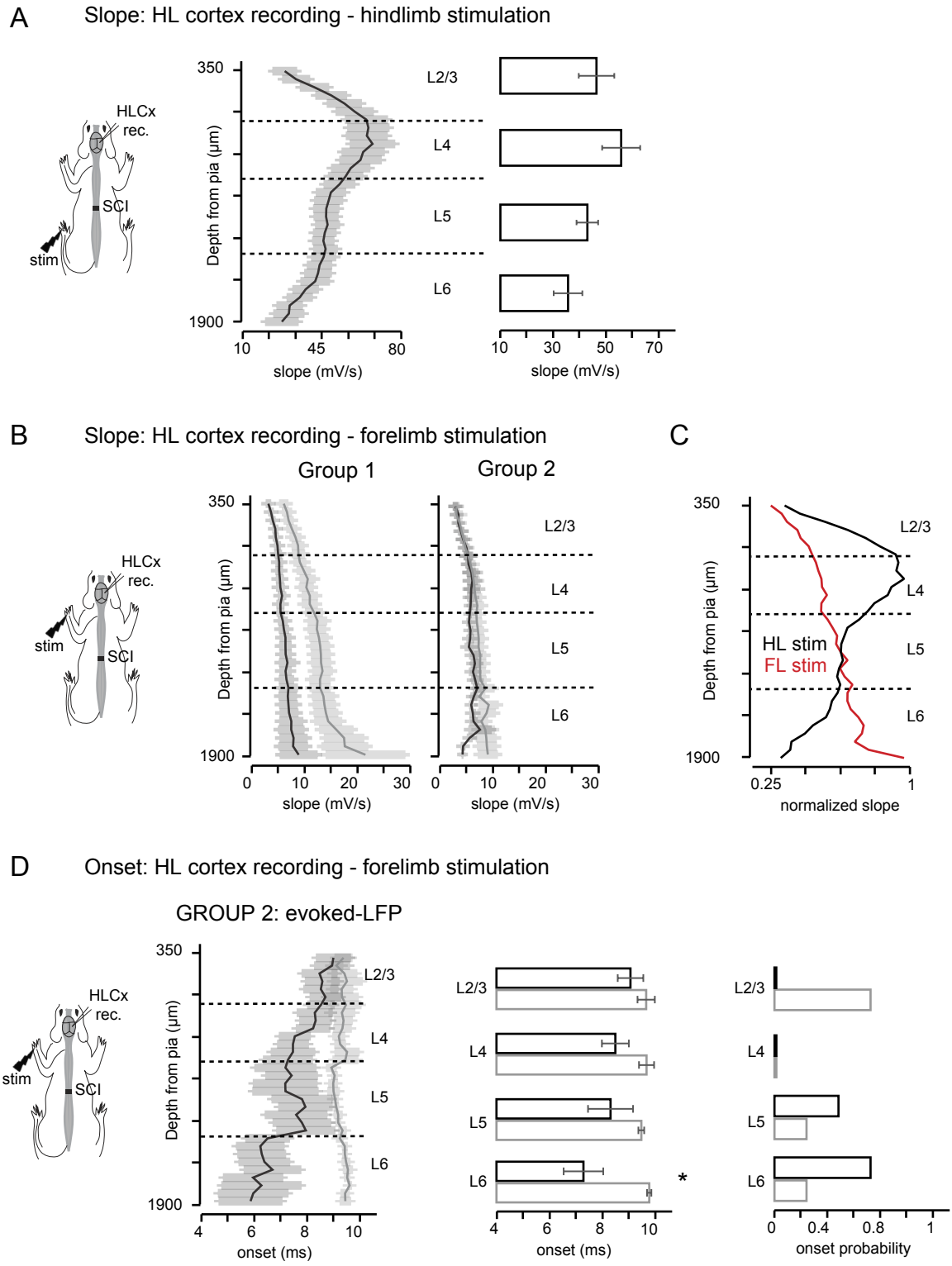

Supplementary Figure 2: Related to Figure 2 and Figure 4, Slope, and onset analysis of the evoked-LFP responses. (A) Top: Averaged slope of evoked LFP from HLCx in response to hindlimb stimulation at 5 mA in control conditions. Bar graph showing the averaged slope values across electrodes within the same layer (n = 5 rats). (B) Averaged slope of evoked-LFP from HLCx in response to forelimb stimulation at 5 mA pre- and post-SCI for animals within Group 1 and 2 (n = 19 and 5 rats, respectively). (C) Normalized slope showing the laminar profile of HLCx responses to hindlimb (black trace) and forelimb stimulation (red trace) at 5 mA. (D) Averaged LFP-onset laminar profile of HLCx in response to forelimb stimulation at 5 mA in Group 2 (n = 5 rats). At left, laminar profile of the whole cortical column. Middle: bar graph showing population averaged onset responses across layers. At right, normalized histogram showing onset probability across layers. Data are mean ± sem. Statistical significance is shown by asterisks for SCI effect (* $p < 0.05$).

Supplementary Table 1: Related to Figure 1, Evoked responses in HLCx by hindlimb and forelimb stimulation. One-way Analysis of Variance (ANOVA) for control responses. Tukey post hoc comparisons are shown for significances $p < 0.05$.

	Limb stimulated	Intensity (mA)	Layer effect	*Post-hoc* Tukey ($p<0.05$)
LFP amplitude	HL	0.5	$F_{(3,89)}=0.9$ $p=0.46$	
		5	$F_{(3,89)}=6.7$ $p<0.001$	L2/3 vs L6; p=0.048 L4 vs L6; p<0.001
	FL	0.5	$F_{(3,92)}=4.1$ $p=0.009$	L2/3 vs L5; p=0.007 L2/3 vs L6; p=0.045
		5	$F_{(3,92)}=12.1$ $p<0.001$	L2/3 vs L5; p<0.001 L2/3 vs L6; p<0.001 L4 vs L6; p=0.024
rMUA area	HL	0.5	$F_{(3,57)}=4.2$ $p=0.009$	L2/3 vs L5; p=0.01 L5 vs L6; p=0.037
		5	$F_{(3,59)}=23$ $p<0.001$	L2/3 vs L4; p=0.03 L2/3 vs L5; p<0.001 L4 vs L5; p<0.001 L5 vs L6; p<0.001
	FL	0.5	$F_{(3,57)}=5.6$ $p=0.002$	L2/3 vs L5; p=0.03 L2/3 vs L6; p=0.008 L4 vs L6; p=0.029
		5	$F_{(3,58)}=7.5$ $p<0.001$	L2/3 vs L5; p=0.005 L2/3 vs L6; p=0.001 L4 vs L6; p=0.015

Supplementary Table 2. Related to Figure 2 and 3, Evoked responses in deafferented HLCx by forelimb stimulation. Two-way repeated measures Analysis of Variance (ANOVA) for comparisons between pre- and post-lesion responses across layers when forelimb was stimulated. Post hoc significance is described just for comparisons between conditions in the same layer (lesion effect).

	Group	mA	Lesion effect	Layer effect	Lesion* Layer effect	*Post-hoc* Tukey
LFP amplitude	All	0.5	$F_{(1,92)}$=51.8 p<0.001	$F_{(3,92)}$=3.2 p=0.026	$F_{(3,92)}$=0.2 p=0.92	L2/3 p=0.055 L4 p=0.006 L5 p=0.003 L6 p=0.015
		5	$F_{(1,91)}$=51.6 p<0.001	$F_{(3,91)}$=10.2 p<0.001	$F_{(3,91)}$=0.3 p=0.81	L2/3 p=0.021 L4 p=0.002 L5 p=0.004 L6 p=0.097
rMUA area	All	0.5	$F_{(1,57)}$=6.5 p=0.014	$F_{(3,57)}$=6.9 p<0.001	$F_{(3,57)}$=1.5 p=0.24	L2/3 p=1 L4 p=1 L5 p=0.393 L6 p=0.223
		5	$F_{(1,59)}$=11.2 p=0.001	$F_{(3,59)}$=10.4 p<0.001	$F_{(3,59)}$=1.6 p=0.19	L2/3 p=1 L4 p=1 L5 p=0.1 L6 p=0.14
LFP amplitude	Group 1 (79%)	0.5	$F_{(1,72)}$=48.5 p<0.001	$F_{(3,72)}$=2.3 p=0.085	$F_{(3,72)}$=0.2 p=0.9	L2/3 p=0.092 L4 p=0.014 L5 p=0.005 L6 p=0.015
		5	$F_{(1,72)}$=125 p<0.001	$F_{(3,72)}$=7 p<0.001	$F_{(3,72)}$=0.5 p=0.68	L2/3 p<0.001 L4 p<0.001 L5 p<0.001 L6 p<0.001
rMUA area	Group 1 (79%)	0.5	$F_{(1,46)}$=2.4 p=0.13	$F_{(3,46)}$=4.3 p=0.009	$F_{(3,46)}$=1.6 p=0.21	
		5	$F_{(1,47)}$=14 p<0.001	$F_{(3,47)}$=8.6 p<0.001	$F_{(3,47)}$=1.91 p=0.14	L2/3 p=1 L4 p=0.97 L5 p=0.044 L6 p=0.086
LFP amplitude	Group 2 (21%)	0.5	$F_{(1,16)}$=4.5 p=0.05	$F_{(3,16)}$=0.8 p=0.5	$F_{(3,16)}$=0.1 p=0.95	
		5	$F_{(1,15)}$=11.3 p=0.004	$F_{(3,15)}$=3.9 p=0.031	$F_{(3,15)}$=1.5 p=0.3	L2/3 p=1 L4 p=0.962 L5 p=0.207 L6 p=0.235
rMUA area	Group 2 (21%)	0.5	$F_{(1,8)}$=3.7 p=0.093	$F_{(3,8)}$=3.8 p=0.056	$F_{(3,8)}$=0.5 p=0.67	
		5	$F_{(1,8)}$=0.6 p=0.46	$F_{(3,8)}$=2.6 p=0.13	$F_{(3,8)}$=0.1 p=0.98	

Supplementary Table 3: Related to Figure 7, Frequency content across layers of HLCx before and immediately after a SCI. Two-way Analysis of Variance (ANOVA) of the relative power spectrum of each band frequency in the spontaneous activity fast transform fourier analysis. Post hoc significance is described just for comparisons between conditions in the same layer (lesion effect). Analysis from Group 1 animals.

	Lesion effect	Layer effect	Lesion*Layer effect	Post hoc Tukey
SWA	$F_{(1,54)}$=5.5 p=0.023	$F_{(3,54)}$=2.1 p=0.136	$F_{(2,54)}$=0.2 p=0.82	L2/3 p=0.95 L4 p =0.49 L5/6 p=0.73
Delta	$F_{(1,54)}$=3.5 p=0.067	$F_{(3,54)}$=0.9 p=0.412	$F_{(2,54)}$=0.3 p=0.76	
Theta	$F_{(1,54)}$=8.9 p=0.004	$F_{(3,54)}$=10.4 p<0.001	$F_{(2,54)}$=0.1 p=0.9	L2/3 p=0.352 L4 p=0.493 L5/6 p=0.741
Alfa	$F_{(1,51)}$=8.9 p=0.02	$F_{(3,51)}$=31.1 p<0.001	$F_{(2,51)}$=0.3 p=0.75	L2/3 p=0.53 L4 p=0.97 L5/6 p=0.58
Beta	$F_{(1,51)}$=2.7 p=0.1	$F_{(3,51)}$=28 p<0.001	$F_{(2,51)}$=0.1 p=0.9	
Low gamma	$F_{(1,51)}$=4.9 p=0.031	$F_{(3,51)}$=15.8 p<0.001	$F_{(2,51)}$=1.3 p=0.27	L2/3 p=0.112 L4 p=0.991 L5/6 p=0.988
High gamma	$F_{(1,51)}$=8.6 p=0.005	$F_{(3,52)}$=11.7 p<0.001	$F_{(2,52)}$=3.3 p=0.046	L2/3 p=0.006 L4 p=0.923 L5 p=0.999